Journal of Computational Physics 349 (2017) 561–581

Contents lists available at ScienceDirect

Journal of Computational Physics

www.elsevier.com/locate/jcp

A high-order CESE scheme with a new divergence-free method for MHD numerical simulation

Yun Yang [a,b,*], Xue-Shang Feng [a,*], Chao-Wei Jiang [c,a]

[a] SIGMA Weather Group, State Key Laboratory of Space Weather, NSSC, Beijing, China
[b] University of Chinese Academy of Sciences, Beijing, China
[c] Institute of Space Science and Applied Technology, Harbin Institute of Technology, Shenzhen, China

ARTICLE INFO

Article history:
Received 23 April 2017
Received in revised form 6 July 2017
Accepted 9 August 2017
Available online 12 August 2017

Keywords:
High-order CESE
MHD
Magnetic field divergence-free
Least-squares method

ABSTRACT

In this paper, we give a high-order space–time conservation element and solution element (CESE) method with a most compact stencil for magneto-hydrodynamics (MHD) equations. This is the first study to extend the second-order CESE scheme to a high order for MHD equations. In the CESE method, the conservative variables and their spatial derivatives are regarded as the independent marching quantities, making the CESE method significantly different from the finite difference method (FDM) and finite volume method (FVM). To utilize the characteristics of the CESE method to the maximum extent possible, our proposed method based on the least-squares method fundamentally keeps the magnetic field divergence-free. The results of some test examples indicate that this new method is very efficient.

1. Introduction

For magneto-hydrodynamics (MHD) numerical simulations, the conservation element and solution element (CESE) scheme has some advantages over the finite volume method (FVM) and finite difference method (FDM) [1]. Particularly for the high-order scheme, the FVM and FDM generally focus on the spatial high order and pay little attention to the temporal high order [2]. Even if the temporal high order is taken into consideration, the FVM and FDM generally use the three- or four-step Runge–Kutta method which is difficult to obtain much higher orders for temporal discretization, such as orders higher than the fifth order. As Balsara et al. [3] reported that, Runge–Kutta time stepping scheme is high cost, for it need to solve Riemann problem at each stage, and if extended to much higher order, it need additional stages, which will make it more expensive. The ADER [3,4] time stepping scheme has obvious advantages than the Runge–Kutta scheme in computation efficiency. But we find the ADER scheme need go through reconstruction, predictor and corrector step, and it doesn't have a single and unique formulation. Especially in the construction step (including the Runge–Kutta scheme), generally need more stencil points for high-order scheme, compared with them, the CESE scheme, is more easily to achieve high-order in time, it only need Taylor series expansion in time with the same stencil as the second-order CESE scheme. As [5] pointed that, the DG scheme has some advantages. In fact, the CESE scheme is similar with the DG finite element, the DG scheme is mainly using finite element to solve the space–time conservation equation while the CESE scheme using a different method to solve it [6]. Andrew et al. [7] and Lishengtai [8] used the Lax–Wendroff method to obtain a temporal

* Corresponding authors.
E-mail addresses: yangyun@spaceweather.ac.cn (Y. Yang), fengx@spaceweather.ac.cn (X.-S. Feng).

http://dx.doi.org/10.1016/j.jcp.2017.08.019
0021-9991/

high order using the FVM method. Their fundamental concept is similar to the CESE method, which combines temporal and spatial discretization to guarantee the simultaneous discretization of any temporal and spatial high order.

The original second-order CESE method was first proposed by Chang et al. [9]. Later, Chang [10] proposed a new any even-order-accuracy CESE method in which the odd-order derivatives were calculated using the central difference method. This is similar to solving first-order derivatives in the original second-order scheme, and even-order derivatives can be obtained by solving the integrated conservation law for the basic high-order derivatives. Bilyeu [11,12] then extended the CESE method to linear and non-linear equation systems. Liu et al. [13] developed an arbitrary-order accuracy CESE scheme in which all the order derivatives were obtained by applying a central difference scheme. Later, Shen et al. [14] extended it to the Euler equation on hybrid grids. Feng et al. [15] applied the original second-order CESE method to the MHD equations. However, thus far, the commonly used method only has second-order accuracy in multidimensional MHD simulations. In the present study, we extend the second-order CESE method to high orders for 2D MHD simulations.

It is well known that, to obtain a high-order scheme using the FVM and FDM methods, such as WENO, PPM, TVD and PNPM scheme, which generally need a larger stencil. This is also the reason why it is difficult to obtain a high-order scheme in numerical simulation. In the present study, we use a compact stencil as in the second-order CESE method to obtain an arbitrary-order accuracy scheme based on the arbitrary-order Taylor expansions in solution elements (SEs).

In contrast to hydrodynamics (HD), for MHD, keeping the magnetic field divergence-free is a great challenge; failure to do so will lead to unphysical forces and numerical instability [16–18]. Some methods have been proposed to keep the magnetic field divergence-free, such as the eight-wave formulation approach [19], the projection method [20], the diffusive method [21], the constrained transport (CT) method [22], the generalized Lagrange multiplier (GLM) method [23] and some others such as the reference [24–27]. In the present study, we take full advantage of the merits of the CESE method and apply the concept of the least-squares method for solving the first-order derivatives, as presented in section 4 in detail.

The remainder of this paper is organized as follows. The MHD governing equations are presented in section 2. Section 3 presents the construction of the high-order CESE method and takes the fourth-order scheme as an example in detail. In section 4, the new method for keeping the magnetic field divergence-free is introduced. Some standard benchmarks are used in the section 5 to check the effectiveness of our new method. Section 6 presents the conclusions.

2. MHD governing equations

In order to exclude the impact of some viscous terms on the accuracy of the high-order scheme, we eliminate the viscous fluxes and source terms and use the ideal MHD equations.

The ideal MHD equations in conservative form in the Cartesian coordinate system are as follows:

$$\frac{\partial \mathbf{U}}{\partial t} + \nabla \cdot \mathbf{F} = 0, \tag{1}$$

where $\mathbf{U} = (u_m) = (\rho, \rho v_x, \rho v_y, \rho v_z, E, B_x, B_y, B_z)^{\mathrm{T}}$, $(m = 1, \cdots, 8)$ is the state vector of the conservative variables. $\mathbf{F}$ denotes the flux vector, which equals $\mathbf{F}$, $(\mathbf{F}, \mathbf{G})$, and $(\mathbf{F}, \mathbf{G}, \mathbf{H})$ for 1, 2, and 3 dimensions, respectively.

$$\mathbf{F} = (f_m) = \begin{pmatrix} \rho v_x \\ \rho v_x^2 + p_0 - B_x^2 \\ \rho v_x v_y - B_x B_y \\ \rho v_x v_z - B_x B_z \\ (E + p) v_x - B_x (v_x B_x + v_y B_y + v_z B_z) \\ 0 \\ v_x B_y - v_y B_x \\ v_x B_z - v_z B_x \end{pmatrix}, \tag{2}$$

$$\mathbf{G} = (g_m) = \begin{pmatrix} \rho v_y \\ \rho v_y v_x - B_y B_x \\ \rho v_y^2 + p_0 - B_y^2 \\ \rho v_y v_z - B_y B_z \\ (E + p) v_y - B_y (v_x B_x + v_y B_y + v_z B_z) \\ v_y B_x - v_x B_y \\ 0 \\ v_y B_z - v_z B_y \end{pmatrix}, \tag{3}$$

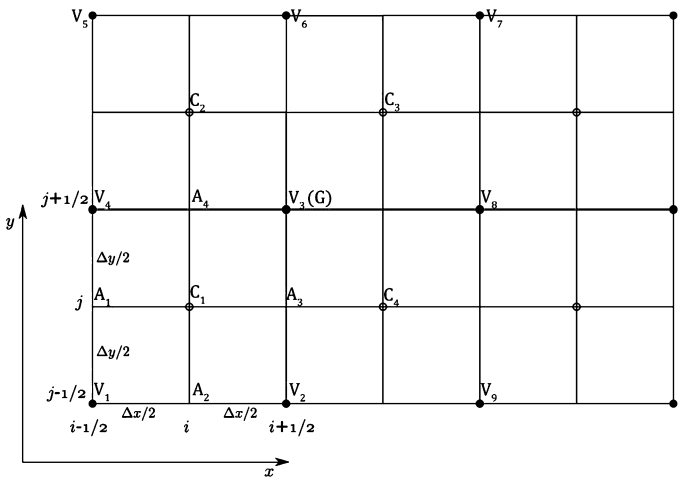

Fig. 1. Projection of the mesh points in E_{2+1} onto the x–y plane.

$$\mathbf{H} = (h_m) = \begin{pmatrix} \rho v_z \\ \rho v_z v_x - B_z B_x \\ \rho v_z v_y - B_z B_y \\ \rho v_z^2 + p_0 - B_z^2 \\ (E+p)v_z - B_z(v_x B_x + v_y B_y + v_z B_z) \\ v_z B_x - v_x B_z \\ v_z B_y - v_y B_z \\ 0 \end{pmatrix}, \tag{4}$$

where $t, \gamma, \rho, E, \boldsymbol{V} = (v_x, v_y, v_z)$, and $\boldsymbol{B} = (B_x, B_y, B_z)$ denote time, the ratio of specific heats, the mass density, total energy, plasma velocity, and magnetic field, respectively. $p = (\gamma - 1)(E - \frac{1}{2}\boldsymbol{V}\cdot\boldsymbol{V} - \frac{1}{2}\boldsymbol{B}\cdot\boldsymbol{B})$ is the gas pressure and $p_0 = p + \boldsymbol{B}^2/2$ is the total pressure.

3. Construction of the high-order CESE scheme

Below, we derive all the formulas in the 2D case, which can be directly extended to the 3D case. Here, we discuss the construction of the fourth-order CESE scheme in detail. The basic concept of the second-order CESE scheme is detailed in Ref. [1,9,14,15], and [28–31].

In the generalized 3D Euclidean space $E_{2+1}(x, y, t)$, which combines the spatial coordinates with the time t, Eq. (1) can be rewritten as

$$\nabla \cdot \mathbf{h}_m = 0, \tag{5}$$

where $\mathbf{h}_m = (f_m, g_m, u_m)$, $(m = 1, \cdots, 8)$ is the space–time flux vector.

By applying Gauss's divergence theorem into Eq. (5) in the 3D space–time domain $E_{2+1}(x, y, t)$, we obtain

$$\oint_{S(V)} \mathbf{h}_m \cdot \mathrm{d}\mathbf{s} = 0, \tag{6}$$

where $S(V)$ is the boundary of any closed space–time region V in $E_{2+1}(x, y, t) \cdot \mathrm{d}\mathbf{s} = (\mathrm{d}\delta)\mathbf{n}$, $\mathrm{d}\delta$ is the area (volume in the 3D case) and $\mathbf{n}$ is the unit outward normal vector of a surface element on $S(V) \cdot \mathbf{h}_m \cdot \mathrm{d}\mathbf{s}$ denotes the total space–time flux leaving the surface element $\mathrm{d}\mathbf{s}$.

As Fig. 1 shows, the space–time domain is discretized by a uniform mesh in Cartesian coordinates. V_i denotes the i-th vertex point, and A_i denotes the i-th mid-point of the element edge. As reported in Ref. [12], for quadrilateral cells, each cell is associated with four basic conservation elements (BCEs), which constitute a compound CE (CCE). In Fig. 1, $\mathrm{V_1V_5V_7V_9}$ is the projection of one CCE, and the projections of four BCEs related to it are $(\mathrm{V_1V_2V_3V_4})$, $(\mathrm{V_3V_4V_5V_6})$, $(\mathrm{V_6V_7V_8V_3})$, and $(\mathrm{V_8V_3V_2V_9})$. C_i is the centroid of the i-th BCE. G is the centroid of CCE. C_i and G are also the solution points of the BCEs and CCE, respectively.

Because the meshes are uniform, the centroids coincide with the center of quadrilaterals. The final solution point G coincides with the vertex point V_3.

There are mainly two kinds of CESE schemes: non-staggered and staggered [14]. In this study, we use the latter. In a full time step, during the first half time step, the solution is updated from the vertexes marked by dots to the cell center

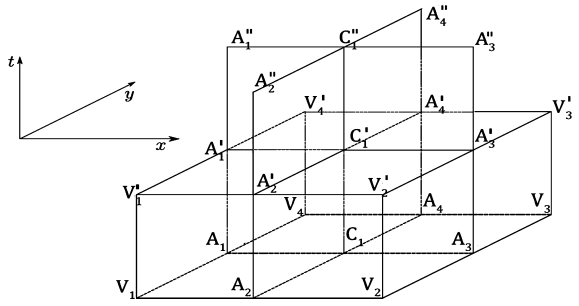

Fig. 2. Definition of CE and SE of point C_1.

marked by hollow circles in Fig. 1. During the second half time step, the solution is updated from the cell center to the vertexes.

Specifically, for a cell point, we first update the solution of its four BCEs, namely C_i, during the first half time step. Following which the values of C_i are used to update the solution of the CCE, namely G, during the second half time step.

For each set of solution points C_i and G, we define a conservation element (CE) and a relevant solution element (SE). Below, we take the point C_1' as an example. As Fig. 2 shows, $CE(C_1')$ is the polygon $V_1V_2V_3V_4V_1'V_2'V_3'V_4'$, and its corresponding $SE(C_1')$ is the union of three planes, $V_1'V_2'V_3'V_4'$, $A_1A_3A_1''A_3''$, and $A_2A_4A_2''A_4''$, which are orthogonal to each other and intersect at C_1'. A_i, V_i, and C_i represent the original solution points at the time level $n-1/2$; A_i', V_i', and C_i' at the time level n; A_i'', V_i'', and C_i'' at time level $n+1/2$, where n is the index for time.

When constructing the CEs, we should guarantee that all the CEs cover the entire space–time domain and that their SEs cover the boundaries of all the CEs but never overlap with each other.

Because the conservation law, i.e., Eq. (6), is suitable for an arbitrary closed space–time domain, the CE we constructed in Fig. 2 will facilitate the derivation of the discrete form of Eq. (6). All the boundaries of the CEs are parallel to the coordinate surfaces, and the normal direction is along the coordinate axis; therefore, on any boundary surface of CEs, there is only one component of the total space–time flux, which makes the integration of space–time fluxes much more convenient, especially for the high-order scheme.

Then, we impose the conservation law, i.e., Eq. (6), on the CE of one point. In each SE, the space–time flux is approximated by Taylor expansion, and the order of Taylor expansion determines the order of the scheme; for example, the first-order Taylor expansion is for second-order scheme. The fourth-order scheme requires the third-order Taylor expansion, and irrespective of the order number, the CEs, SEs, and stencils are always the same as in the second-order scheme, which is one advantage of this type of high-order CESE scheme. Below, we still consider the point C_1 as an example.

By imposing Eq. (6) on the conservation element of C_1, we obtain

$$\oint_{S(CE(C_1))} \mathbf{h}_m \cdot d\mathbf{s} = \oint_{S(V_1V_2V_3V_4V_1'V_2'V_3'V_4')} \mathbf{h}_m \cdot d\mathbf{s} = 0. \tag{7}$$

In a half time step, the integration $\oint_{S(V_1V_2V_3V_4V_1'V_2'V_3'V_4')} \mathbf{h}_m \cdot d\mathbf{s}$ in Eq. (7) includes three parts: 1) integrating over the bottom surface $V_1V_2V_3V_4$;

2) integrating over the side surfaces $V_1V_1'V_2'V_2$, $V_2V_2'V_3'V_3$, $V_3V_3'V_4'V_4$, and $V_4V_4'V_1'V_1$;

3) integrating over the top surface $V_1'V_2'V_3'V_4'$.

Below, we present the integration of space–time fluxes over each boundary surface of CEs. All the notations used below such as u_{mxy}, f_{mxt}, m denotes m-th component of eight conservative variables or flux. x, y, t denote their partial derivatives with respect to space or time.

1) Integration over the bottom surface of CEs

Only the space–time flux **U** passes through the bottom surface. The bottom surface integration will be split into four parts. On each part, u_m is approximated by the third-order Taylor expansion at the points V_1, V_2, V_3, V_4. In Fig. 2, on the part $V_1A_2C_1A_1$, u_m is approximated by the third-order Taylor expansion at the point V_1

$$\int_{(i-\frac{1}{2})\Delta x}^{i\Delta x}\int_{(j-\frac{1}{2})\Delta y}^{j\Delta y} \Big\{(u_m)_{V_1} + (u_{mx})_{V_1}\Big[x-\Big(i-\frac{1}{2}\Big)\Delta x\Big] + (u_{my})_{V_1}\Big[y-\Big(j-\frac{1}{2}\Big)\Delta y\Big]$$
$$+\frac{1}{2}(u_{mxx})_{V_1}\Big[x-\Big(i-\frac{1}{2}\Big)\Delta x\Big]^2 + \frac{1}{2}(u_{myy})_{V_1}\Big[y-\Big(j-\frac{1}{2}\Big)\Delta y\Big]^2$$
$$+\frac{1}{2}\big[(u_{mxy})_{V_1} + (u_{myx})_{V_1}\big]\Big[x-\Big(i-\frac{1}{2}\Big)\Delta x\Big]\Big[y-\Big(j-\frac{1}{2}\Big)\Delta y\Big]$$

$$
\begin{aligned}
&+\frac{1}{6}(u_{mxxx})_{V_1}\left[x-\left(i-\frac{1}{2}\right)\Delta x\right]^3+\frac{1}{6}(u_{myyy})_{V_1}\left[y-\left(j-\frac{1}{2}\right)\Delta y\right]^3\\
&+\frac{1}{6}\left[(u_{myyx})_{V_1}+(u_{myxy})_{V_1}+(u_{mxyy})_{V_1}\right]\left[y-\left(j-\frac{1}{2}\right)\Delta y\right]^2\left[x-\left(i-\frac{1}{2}\right)\Delta x\right]\\
&+\frac{1}{6}\left[(u_{mxxy})_{V_1}+(u_{mxyx})_{V_1}+(u_{myxx})_{V_1}\right]\left[x-\left(i-\frac{1}{2}\right)\Delta x\right]^2\left[y-\left(j-\frac{1}{2}\right)\Delta y\right]\Bigg\}dxdy\\
=&\frac{\Delta x\Delta y}{4}\Bigg\{(u_m)_{V_1}+(u_{mx})_{V_1}\frac{\Delta x}{4}+(u_{my})_{V_1}\frac{\Delta y}{4}+(u_{mxx})_{V_1}\frac{\Delta x^2}{24}+(u_{myy})_{V_1}\frac{\Delta y^2}{24}\\
&+\left[(u_{mxy})_{V_1}+(u_{myx})_{V_1}\right]\frac{\Delta x\Delta y}{32}+(u_{mxxx})_{V_1}\frac{\Delta x^3}{192}+(u_{myyy})_{V_1}\frac{\Delta y^3}{192}\\
&+\left[(u_{myyx})_{V_1}+(u_{myxy})_{V_1}+(u_{mxyy})_{V_1}\right]\frac{\Delta y^2\Delta x}{288}\\
&+\left[(u_{mxxy})_{V_1}+(u_{mxyx})_{V_1}+(u_{myxx})_{V_1}\right]\frac{\Delta x^2\Delta y}{288}\Bigg\}.
\end{aligned}
$$

On the part $V_2A_2C_1A_3$, u_m is approximated by the third-order Taylor expansion at the point V_2

$$
\begin{aligned}
&\int_{i\Delta x}^{(i+\frac{1}{2})\Delta x}\int_{(j-\frac{1}{2})\Delta y}^{j\Delta y}\Bigg\{(u_m)_{V_2}+(u_{mx})_{V_2}\left[x-\left(i+\frac{1}{2}\right)\Delta x\right]+(u_{my})_{V_2}\left[y-\left(j-\frac{1}{2}\right)\Delta y\right]\\
&+\frac{1}{2}(u_{mxx})_{V_2}\left[x-\left(i+\frac{1}{2}\right)\Delta x\right]^2+\frac{1}{2}(u_{myy})_{V_2}\left[y-\left(j-\frac{1}{2}\right)\Delta y\right]^2\\
&+\frac{1}{2}\left[(u_{mxy})_{V_2}+(u_{myx})_{V_2}\right]\left[x-\left(i+\frac{1}{2}\right)\Delta x\right]\left[y-\left(j-\frac{1}{2}\right)\Delta y\right]\\
&+\frac{1}{6}(u_{mxxx})_{V_2}\left[x-\left(i+\frac{1}{2}\right)\Delta x\right]^3+\frac{1}{6}(u_{myyy})_{V_2}\left[y-\left(j-\frac{1}{2}\right)\Delta y\right]^3\\
&+\frac{1}{6}\left[(u_{myyx})_{V_2}+(u_{myxy})_{V_2}+(u_{mxyy})_{V_2}\right]\left[x-\left(i+\frac{1}{2}\right)\Delta x\right]\left[y-\left(j-\frac{1}{2}\right)\Delta y\right]^2\\
&+\frac{1}{6}\left[(u_{mxxy})_{V_2}+(u_{mxyx})_{V_2}+(u_{myxx})_{V_2}\right]\left[x-\left(i+\frac{1}{2}\right)\Delta x\right]^2\left[y-\left(j-\frac{1}{2}\right)\Delta y\right]\Bigg\}dxdy\\
=&\frac{\Delta x\Delta y}{4}\Bigg\{(u_m)_{V_2}-(u_{mx})_{V_2}\frac{\Delta x}{4}+(u_{my})_{V_2}\frac{\Delta y}{4}+(u_{mxx})_{V_2}\frac{\Delta x^2}{24}+(u_{myy})_{V_2}\frac{\Delta y^2}{24}\\
&-\left[(u_{mxy})_{V_2}+(u_{myx})_{V_2}\right]\frac{\Delta x\Delta y}{32}-(u_{mxxx})_{V_2}\frac{\Delta x^3}{192}+(u_{myyy})_{V_2}\frac{\Delta y^3}{192}\\
&-\left[(u_{myyx})_{V_2}+(u_{myxy})_{V_2}+(u_{mxyy})_{V_2}\right]\frac{\Delta y^2\Delta x}{288}\\
&+\left[(u_{mxxy})_{V_2}+(u_{mxyx})_{V_2}+(u_{myxx})_{V_2}\right]\frac{\Delta x^2\Delta y}{288}\Bigg\}.
\end{aligned}
$$

On the part $V_3A_3C_1A_4$,

$$
\begin{aligned}
&\int_{i\Delta x}^{(i+\frac{1}{2})\Delta x}\int_{j\Delta y}^{(j+\frac{1}{2})\Delta y}\Bigg\{(u_m)_{V_3}+(u_{mx})_{V_3}\left[x-\left(i+\frac{1}{2}\right)\Delta x\right]+(u_{my})_{V_3}\left[y-\left(j+\frac{1}{2}\right)\Delta y\right]\\
&+\frac{1}{2}(u_{mxx})_{V_3}\left[x-\left(i+\frac{1}{2}\right)\Delta x\right]^2+\frac{1}{2}(u_{myy})_{V_3}\left[y-\left(j+\frac{1}{2}\right)\Delta y\right]^2
\end{aligned}
$$

$$
\begin{aligned}
&+\frac{1}{2}\left[(u_{mxy})_{V_3}+(u_{myx})_{V_3}\right]\left[x-\left(i+\frac{1}{2}\right)\Delta x\right]\left[y-\left(j+\frac{1}{2}\right)\Delta y\right]\\
&+\frac{1}{6}(u_{mxxx})_{V_3}\left[x-\left(i+\frac{1}{2}\right)\Delta x\right]^3+\frac{1}{6}(u_{myyy})_{V_3}\left[y-\left(j+\frac{1}{2}\right)\Delta y\right]^3\\
&+\frac{1}{6}\left[(u_{myyx})_{V_3}+(u_{myxy})_{V_3}+(u_{mxyy})_{V_3}\right]\left[x-\left(i+\frac{1}{2}\right)\Delta x\right]\left[y-\left(j+\frac{1}{2}\right)\Delta y\right]^2\\
&+\frac{1}{6}\left[(u_{mxxy})_{V_3}+(u_{mxyx})_{V_3}+(u_{myxx})_{V_3}\right]\left[x-\left(i+\frac{1}{2}\right)\Delta x\right]^2\left[y-\left(j+\frac{1}{2}\right)\Delta y\right]\Bigg\}dxdy\\
=&\frac{\Delta x\Delta y}{4}\Bigg\{(u_m)_{V_3}-(u_{mx})_{V_3}\frac{\Delta x}{4}-(u_{my})_{V_3}\frac{\Delta y}{4}+(u_{mxx})_{V_3}\frac{1}{24}\Delta x^2+(u_{myy})_{V_3}\frac{1}{24}\Delta y^2\\
&+\left[(u_{mxy})_{V_3}+(u_{myx})_{V_3}\right]\frac{\Delta x\Delta y}{32}-(u_{mxxx})_{V_3}\frac{\Delta x^3}{192}-(u_{myyy})_{V_3}\frac{\Delta y^3}{192}\\
&-\left[(u_{myyx})_{V_3}+(u_{myxy})_{V_3}+(u_{mxyy})_{V_3}\right]\frac{\Delta y^2\Delta x}{288}\\
&-\left[(u_{mxxy})_{V_3}+(u_{mxyx})_{V_3}+(u_{myxx})_{V_3}\right]\frac{\Delta x^2\Delta y}{288}\Bigg\}.
\end{aligned}
$$

On the part $V_4A_1C_1A_4$,

$$
\begin{aligned}
&\int_{(i-\frac{1}{2})\Delta x}^{i\Delta x}\int_{j\Delta y}^{(j+\frac{1}{2})\Delta y}\Bigg\{(u_m)_{V_4}+(u_{mx})_{V_4}\left[x-\left(i-\frac{1}{2}\right)\Delta x\right]+(u_{my})_{V_4}\left[y-\left(j+\frac{1}{2}\right)\Delta y\right]\\
&+\frac{1}{2}(u_{mxx})_{V_4}\left[x-\left(i-\frac{1}{2}\right)\Delta x\right]^2+\frac{1}{2}(u_{myy})_{V_4}\left[y-\left(j+\frac{1}{2}\right)\Delta y\right]^2\\
&+\frac{1}{2}\left[(u_{mxy})_{V_4}+(u_{myx})_{V_4}\right]\left[x-\left(i-\frac{1}{2}\right)\Delta x\right]\left[y-\left(j+\frac{1}{2}\right)\Delta y\right]\\
&+\frac{1}{6}(u_{mxxx})_{V_4}\left[x-\left(i-\frac{1}{2}\right)\Delta x\right]^3+\frac{1}{6}(u_{myyy})_{V_4}\left[y-\left(j+\frac{1}{2}\right)\Delta y\right]^3\\
&+\frac{1}{6}\left[(u_{myyx})_{V_4}+(u_{myxy})_{V_4}+(u_{mxyy})_{V_4}\right]\left[x-\left(i-\frac{1}{2}\right)\Delta x\right]\left[y-\left(j+\frac{1}{2}\right)\Delta y\right]^2\\
&+\frac{1}{6}\left[(u_{mxxy})_{V_4}+(u_{mxyx})_{V_4}+(u_{myxx})_{V_4}\right]\left[x-\left(i-\frac{1}{2}\right)\Delta x\right]^2\left[y-\left(j+\frac{1}{2}\right)\Delta y\right]\Bigg\}dxdy\\
=&\frac{\Delta x\Delta y}{4}\Bigg\{(u_m)_{V_4}+(u_{mx})_{V_4}\frac{\Delta x}{4}-(u_{my})_{V_4}\frac{\Delta y}{4}+(u_{mxx})_{V_4}\frac{\Delta x^2}{24}+(u_{myy})_{V_4}\frac{\Delta y^2}{24}\\
&-\left[(u_{mxy})_{V_4}+(u_{myx})_{V_4}\right]\frac{\Delta x\Delta y}{32}+(u_{mxxx})_{V_4}\frac{\Delta x^3}{192}-(u_{myyy})_{V_4}\frac{\Delta y^3}{192}\\
&+\left[(u_{myyx})_{V_4}+(u_{myxy})_{V_4}+(u_{mxyy})_{V_4}\right]\frac{\Delta y^2\Delta x}{288}\\
&-\left[(u_{mxxy})_{V_4}+(u_{mxyx})_{V_4}+(u_{myxx})_{V_4}\right]\frac{\Delta x^2\Delta y}{288}\Bigg\}.
\end{aligned}
$$

2) Integration over the side surfaces of CEs

Only the space–time flux **G** passes through the two side surfaces in the direction of the x axis, $V_1V_1'V_2'V_2$ and $V_3V_3'V_4'V_4$. Only the space–time flux **F** passes through the two side surfaces in the direction of the y axis, $V_1V_1'V_4'V_4$ and $V_2V_2'V_3'V_3$.

Each side surface is split into two parts. On each part, the fluxes are approximated by the third-order Taylor expansion at the near solution point. For example, the surface $V_1V_1'V_4'V_4$ is split into $V_1V_1'A_1'A_1$ and $A_1A_1'V_4'V_4$. On $V_1V_1'A_1'A_1$, f_m is approximated at V_1; on $A_1A_1'V_4'V_4$, f_m is approximated at V_4.

On the surface $V_1V_1'V_4'V_4$, $x=(i-\frac{1}{2})\Delta x$ is a constant; therefore, all the integration terms containing Δx are zero.

The integration on the surface $V_1V_1'A_1'A_1$ is as follows:

$$
\begin{aligned}
&\int_{(j-\frac{1}{2})\Delta y}^{j\Delta y}\int_{(k-\frac{1}{2})\Delta t}^{k\Delta t}\Big\{(f_m)_{V_1}+(f_{my})_{V_1}\Big[y-\Big(j-\frac{1}{2}\Big)\Delta y\Big]+(f_{mt})_{V_1}\Big[t-\Big(k-\frac{1}{2}\Big)\Delta t\Big]\\
&\quad+\frac{1}{2}(f_{myy})_{V_1}\Big[y-\Big(j-\frac{1}{2}\Big)\Delta y\Big]^2+\frac{1}{2}(f_{mtt})_{V_1}\Big[t-\Big(k-\frac{1}{2}\Big)\Delta t\Big]^2\\
&\quad+(f_{myt})_{V_1}\Big[y-\Big(j-\frac{1}{2}\Big)\Delta y\Big]\Big[t-\Big(k-\frac{1}{2}\Big)\Delta t\Big]\\
&\quad+\frac{1}{6}(f_{myyy})_{V_1}\Big[y-\Big(j-\frac{1}{2}\Big)\Delta y\Big]^3+\frac{1}{6}(f_{mttt})_{V_1}\Big[t-\Big(k-\frac{1}{2}\Big)\Delta t\Big]^3\\
&\quad+\frac{1}{2}(f_{myyt})_{V_1}\Big[y-\Big(j-\frac{1}{2}\Big)\Delta y\Big]^2\Big[t-\Big(k-\frac{1}{2}\Big)\Delta t\Big]\\
&\quad+\frac{1}{2}(f_{mytt})_{V_1}\Big[y-\Big(j-\frac{1}{2}\Big)\Delta y\Big]\Big[t-\Big(k-\frac{1}{2}\Big)\Delta t\Big]^2\Big\}dydt\\
&=\frac{\Delta y\Delta t}{4}\Big\{(f_m)_{V_1}+(f_{my})_{V_1}\frac{\Delta y}{4}+(f_{mt})_{V_1}\frac{\Delta t}{4}+(f_{myy})_{V_1}\frac{\Delta y^2}{24}+(f_{mtt})_{V_1}\frac{\Delta t^2}{24}\\
&\quad+(f_{myt})_{V_1}\frac{\Delta y\Delta t}{16}+(f_{myyy})_{V_1}\frac{\Delta y^3}{192}+(f_{mttt})_{V_1}\frac{\Delta t^3}{192}\\
&\quad+(f_{myyt})_{V_1}\frac{\Delta y^2\Delta t}{96}+(f_{mytt})_{V_1}\frac{\Delta y\Delta t^2}{96}\Big\}.
\end{aligned}
$$

On the surface $A_1A_1'V_4'V_4$,

$$
\begin{aligned}
&\int_{j\Delta y}^{(j+\frac{1}{2})\Delta y}\int_{(k-\frac{1}{2})\Delta t}^{k\Delta t}\Big\{(f_m)_{V_4}+(f_{my})_{V_4}\Big[y-\Big(j+\frac{1}{2}\Big)\Delta y\Big]+(f_{mt})_{V_4}\Big[t-\Big(k-\frac{1}{2}\Big)\Delta t\Big]\\
&\quad+\frac{1}{2}(f_{myy})_{V_4}\Big[y-\Big(j+\frac{1}{2}\Big)\Delta y\Big]^2+\frac{1}{2}(f_{mtt})_{V_4}\Big[t-\Big(k-\frac{1}{2}\Big)\Delta t\Big]^2\\
&\quad+(f_{myt})_{V_4}\Big[y-\Big(j+\frac{1}{2}\Big)\Delta y\Big]\Big[t-\Big(k-\frac{1}{2}\Big)\Delta t\Big]\\
&\quad+\frac{1}{6}(f_{myyy})_{V_4}\Big[y-\Big(j+\frac{1}{2}\Big)\Delta y\Big]^3+\frac{1}{6}(f_{mttt})_{V_4}\Big[t-\Big(k-\frac{1}{2}\Big)\Delta t\Big]^3\\
&\quad+\frac{1}{2}(f_{myyt})_{V_4}\Big[y-\Big(j+\frac{1}{2}\Big)\Delta y\Big]^2\Big[t-\Big(k-\frac{1}{2}\Big)\Delta t\Big]\\
&\quad+\frac{1}{2}(f_{mytt})_{V_4}\Big[y-\Big(j+\frac{1}{2}\Big)\Delta y\Big]\Big[t-\Big(k-\frac{1}{2}\Big)\Delta t\Big]^2\Big\}dydt\\
&=\frac{\Delta y\Delta t}{4}\Big\{(f_m)_{V_4}-(f_{my})_{V_4}\frac{\Delta y}{4}+(f_{mt})_{V_4}\frac{\Delta t}{4}+(f_{myy})_{V_4}\frac{\Delta y^2}{24}+(f_{mtt})_{V_4}\frac{\Delta t^2}{24}\\
&\quad-(f_{myt})_{V_4}\frac{\Delta y\Delta t}{16}-(f_{myyy})_{V_4}\frac{\Delta y^3}{192}+(f_{mttt})_{V_4}\frac{\Delta t^3}{192}\\
&\quad+(f_{myyt})_{V_4}\frac{\Delta y^2\Delta t}{96}-(f_{mytt})_{V_4}\frac{\Delta y\Delta t^2}{96}\Big\}.
\end{aligned}
$$

On the surface $V_2V_2'V_3'V_3$, $x=(i+\frac{1}{2})\Delta x$ is also a constant. Therefore, the integration on the surfaces $V_2V_2'A_3'A_3$ and $A_3A_3'V_3'V_3$ is similar to that on $V_1V_1'A_1'A_1$ and $A_1A_1'V_4'V_4$, except that the outward normal direction is opposite; the fluxes are approximated at points V_2 and V_3, respectively.

On the two surfaces in the direction of the x axis, $V_1V_1'V_2'V_2$ and $V_3V_3'V_4'V_4$, $y=(j-\frac{1}{2})\Delta y$ and $y=(j+\frac{1}{2})\Delta y$ are constants; therefore, on these two surfaces, all the integration terms containing Δy are zero. The final integration form is similar to those on the surface in the direction of y axis, with f_m replaced by g_m and y by x.

3) Integration over the top surface of CEs

Only the space–time flux **U** passes through the top surface, but it is different from the bottom surface in that the flux is approximated at the solution point C_1' on the entire top surface.

$$\begin{aligned}
&\int_{(i-\frac{1}{2})\Delta x}^{(i+\frac{1}{2})\Delta x}\int_{(j-\frac{1}{2})\Delta y}^{(j+\frac{1}{2})\Delta y}\Big\{(u_m)_{C_1'}+(u_{mx})_{C_1'}[x-i\Delta x]+(u_{my})_{C_1'}[y-j\Delta y]\\
&\quad+\frac{1}{2}(u_{mxx})_{C_1'}[x-i\Delta x]^2+\frac{1}{2}(u_{myy})_{C_1'}[y-j\Delta y]^2\\
&\quad+\frac{1}{2}\big[(u_{mxy})_{C_1'}+(u_{myx})_{C_1'}\big][x-i\Delta x][y-j\Delta y]\\
&\quad+\frac{1}{6}(u_{mxxx})_{C_1'}[x-i\Delta x]^3+\frac{1}{6}(u_{myyy})_{C_1'}[y-j\Delta y]^3\\
&\quad+\frac{1}{6}\big[(u_{myyx})_{C_1'}+(u_{myxy})_{C_1'}+(u_{mxyy})_{C_1'}\big][x-i\Delta x][y-j\Delta y]^2\\
&\quad+\frac{1}{6}\big[(u_{myxx})_{C_1'}+(u_{mxyx})_{C_1'}+(u_{mxxy})_{C_1'}\big][x-i\Delta x]^2[y-j\Delta y]\Big\}dxdy\\
&=\Delta x\Delta y\left\{(u_m)_{C_1'}+(u_{mxx})_{C_1'}\frac{\Delta x^2}{24}+(u_{myy})_{C_1'}\frac{\Delta y^2}{24}\right\}.
\end{aligned}$$

After the integration over all the boundary surfaces of CEs, we obtain the updated variables $\mathbf{U}_{updated}$ as follows:

$$\mathbf{U}_{updated}=\Big(\sum I_{bottom}-\sum I_{side}-\sum I_{top}^{*}\Big)/\text{Area\_top\_surface}, \tag{8}$$

where I_{bottom} and I_{side} are the space–time flux integration on the bottom and side surface of CEs, respectively. I_{top}^{*} is the high-order part of flux integration on the top surface.

The form of Eq. (8) for the fourth-order scheme is as follows:

$$\begin{aligned}
(u_m)_{i,j}^{n}=\frac{1}{\Delta x\Delta y}\sum_{l=1}^{4}\Bigg\{&\frac{\Delta x\Delta y}{4}\left\{(u_m)_l^{n-1/2}+(u_{mx})_l^{n-1/2}\left(k_x\frac{\Delta x}{4}\right)+(u_{my})_l^{n-1/2}\left(k_y\frac{\Delta y}{4}\right)\right.\\
&+\frac{1}{24}\big[(u_{mxx})_l^{n-1/2}(k_x\Delta x)^2+(u_{myy})_l^{n-1/2}(k_y\Delta y)^2\big]\\
&+\frac{1}{32}\big[(u_{mxy})_l^{n-1/2}+(u_{myx})_l^{n-1/2}\big](k_x\Delta x)(k_y\Delta y)\\
&+\frac{1}{192}\big[(u_{mxxx})_l^{n-1/2}(k_x\Delta x)^3+(u_{myyy})_l^{n-1/2}(k_y\Delta y)^3\big]\\
&+\frac{(k_x\Delta x)^2(k_y\Delta y)}{288}\big[(u_{mxxy})_l^{n-1/2}+(u_{mxyx})_l^{n-1/2}+(u_{myxx})_l^{n-1/2}\big]\\
&\left.+\frac{(k_y\Delta y)^2(k_x\Delta x)}{288}\big[(u_{myyx})_l^{n-1/2}+(u_{myxy})_l^{n-1/2}+(u_{mxyy})_l^{n-1/2}\big]\right\}\\
&+k_x\frac{\Delta y\Delta t}{4}\left\{(f_m)_l^{n-1/2}+(f_{my})_l^{n-1/2}\left(k_y\frac{\Delta y}{4}\right)+(f_{mt})_l^{n-1/2}\left(\frac{\Delta t}{4}\right)\right.\\
&+\frac{1}{24}\big[(f_{mtt})_l^{n-1/2}(\Delta t)^2+(f_{myy})_l^{n-1/2}(k_y\Delta y)^2\big]\\
&+\frac{1}{16}(f_{myt})_l^{n-1/2}(k_y\Delta y)\Delta t\\
&+\frac{1}{192}\big[(f_{myyy})_l^{n-1/2}(k_y\Delta y)^3+(f_{mttt})_l^{n-1/2}(\Delta t)^3\big]\\
&\left.+\frac{1}{96}\big[(f_{myyt})_l^{n-1/2}(k_y\Delta y)^2\Delta t+(f_{mytt})_l^{n-1/2}(k_y\Delta y)(\Delta t)^2\big]\right\}\\
&+k_y\frac{\Delta x\Delta t}{4}\left\{(g_m)_l^{n-1/2}+(g_{mx})_l^{n-1/2}\left(k_x\frac{\Delta x}{4}\right)+(g_{mt})_l^{n-1/2}\left(\frac{\Delta t}{4}\right)\right.
\end{aligned}$$

$$+\frac{1}{24}\left[(g_{mtt})_l^{n-1/2}(\Delta t)^2+(g_{mxx})_l^{n-1/2}(k_x\Delta x)^2\right]$$
$$+\frac{1}{16}(g_{mxt})_l^{n-1/2}(k_x\Delta x)\Delta t$$
$$+\frac{1}{192}\left[(g_{mxxx})_l^{n-1/2}(k_x\Delta x)^3+(g_{mttt})_l^{n-1/2}(\Delta t)^3\right]$$
$$+\frac{1}{96}\left[(g_{mxxt})_l^{n-1/2}(k_x\Delta x)^2\Delta t+(g_{mxtt})_l^{n-1/2}(k_x\Delta x)(\Delta t)^2\right]\Bigg\}\Bigg\rangle$$
$$-\frac{1}{24}\left[(u_{mxx})_{C_1}^n(\Delta x)^2+(u_{myy})_{C_1}^n(\Delta y)^2\right]. \tag{9}$$

In the above equation, $m=1,2,\cdots,8$ represent eight equations, and $l=1,2,3,4$ represent four solution points V_1, V_2, V_3, V_4, respectively. k_x, k_y is -1 or 1, as determined by the position of the four solution points V_1, V_2, V_3, V_4 relative to the center point C_1.

The derivatives of flux **F** and **G** with respect to x, y, and t can be obtained according to the chain rule.

$$\frac{\partial T_m}{\partial \phi_1}=\sum_{p=1}^{8}\frac{\partial T_m}{\partial u_p}\frac{\partial u_p}{\partial \phi_1}, \tag{10}$$

where T_m represents f_m or g_m and $\phi_1=\{x,y,t\}$.

By using the chain rule for Eq. (10), we can obtain the second-order derivatives as follows:

$$\frac{\partial^2 T_m}{\partial \phi_1\partial \phi_2}=\sum_{p=1}^{8}\frac{\partial T_m}{\partial u_p}\frac{\partial^2 u_p}{\partial \phi_1\partial \phi_2}+\sum_{p=1}^{8}\sum_{q=1}^{8}\frac{\partial^2 T_m}{\partial u_p\partial u_q}\frac{\partial u_p}{\partial \phi_1}\frac{\partial u_q}{\partial \phi_2}, \tag{11}$$

where $(\phi_1,\phi_2)=\{(x,x),(y,y),(t,t),(x,y),(y,x),(x,t),(y,t)\}$.

Similarly, by using the chain rule for Eq. (11), we can obtain the third-order derivatives as follows:

$$\begin{aligned}\frac{\partial^3 T_m}{\partial \phi_1\partial \phi_2\partial \phi_3}=&\sum_{p=1}^{8}\frac{\partial T_m}{\partial u_p}\frac{\partial^3 u_p}{\partial \phi_1\partial \phi_2\partial \phi_3}\\&+\sum_{p=1}^{8}\sum_{q=1}^{8}\frac{\partial^2 T_m}{\partial u_p\partial u_q}\left(\frac{\partial^2 u_p}{\partial \phi_1\partial \phi_2}\frac{\partial u_q}{\partial \phi_3}+\frac{\partial^2 u_p}{\partial \phi_1\partial \phi_3}\frac{\partial u_q}{\partial \phi_2}+\frac{\partial^2 u_p}{\partial \phi_2\partial \phi_3}\frac{\partial u_q}{\partial \phi_1}\right)\\&+\sum_{p=1}^{8}\sum_{q=1}^{8}\sum_{r=1}^{8}\frac{\partial^3 T_m}{\partial u_p\partial u_q\partial u_r}\frac{\partial u_p}{\partial \phi_1}\frac{\partial u_q}{\partial \phi_2}\frac{\partial u_r}{\partial \phi_3},\end{aligned} \tag{12}$$

where

$$\begin{aligned}(\phi_1,\phi_2,\phi_3)=\big\{&(x,x,x),(x,x,y),(x,y,x),(x,y,y),(y,x,x),\\&(y,x,y),(y,y,x),(y,y,y),(x,x,t),(x,y,t),\\&(y,x,t),(y,y,t),(x,t,t),(y,t,t),(t,t,t)\big\}.\end{aligned}$$

In the same way, we can get much higher-order derivatives.

Bilyeu [12] reported that, at some points, the alternate rule of differentiation does not hold. Therefore, here we regard $\frac{\partial^2 u}{\partial x\partial y}$ and $\frac{\partial^2 u}{\partial y\partial x}$ as different variables.

In Eq. (10), Eq. (11), and Eq. (12), we first need to obtain the Jacobian matrices $\frac{\partial T_m}{\partial u_p}$, $\frac{\partial^2 T_m}{\partial u_p\partial u_q}$, $\frac{\partial^3 T_m}{\partial u_p\partial u_q\partial u_r}$, where $T_m=f_m$ or g_m. The Jacobian matrices can be obtained by directly taking the derivative of flux with respect to every conservative variable in sequence, but for MHD equations, this process is cumbersome (we have attempted this method), especially when adding the second- and third-order Jacobian matrices. We used the symbolic math of Matlab to obtain the Jacobian matrices.

In the actual application, for the derivation with respect to time t, we should note the solving sequence. Solving in the following sequence will be economic and effective.

After obtaining f_{mx} and g_{my}, according to the conservation law expressed by Eq. (1), we can obtain u_{mt} as

$$u_{mt}=-f_{mx}-g_{my}. \tag{13}$$

By taking the derivative of Eq. (13) with respect to x or y, we obtain

$$u_{mxt} = -f_{mxx} - g_{myx}, \tag{14}$$

$$u_{myt} = -f_{mxy} - g_{myy}. \tag{15}$$

Then, according to Eq. (10) and Eq. (11), we obtain $f_{mt}, g_{mt}, f_{mxt}, g_{mxt}, f_{myt}, g_{myt}$.

By taking the derivative of Eq. (13) with respect to t, we obtain

$$u_{mtt} = -f_{mxt} - g_{myt}. \tag{16}$$

Then, by taking the derivative of Eq. (16) with respect to x or y, we obtain

$$u_{mxtt} = -f_{mxxt} - g_{myxt}, \tag{17}$$

$$u_{mytt} = -f_{mxyt} - g_{myyt}. \tag{18}$$

According to Eq. (11) and Eq. (12), we obtain $f_{mtt}, g_{mtt}, f_{mxtt}, g_{mxtt}, f_{mytt}, g_{mytt}$.

Then, by taking the derivative of Eq. (16) with respect to t, we obtain

$$u_{mttt} = -f_{mxtt} - g_{mytt}. \tag{19}$$

Finally, according to Eq. (12) we obtain f_{mttt}, g_{mttt}.

From Eq. (13)–Eq. (19), we can find that all the derivatives with respect to t of conservative variables can be obtained through the derivatives of flux f_m and g_m. Moreover, the derivatives of flux f_m and g_m can be obtained from the derivatives of conservative variables with respect to x or y. Therefore, at the end, to update the conservative variables of Eq. (9), we only need to obtain the derivatives of conservative variables with respect to x or y for all orders. For example, for the fourth-order scheme, we need to update the values of $u_{mx}, u_{my}, u_{mxx}, u_{mxy}, u_{myx}, u_{myy}, u_{mxxx}, u_{mxxy}, u_{mxyx}, u_{mxyy}, u_{myxx}, u_{myxy}, u_{myyx}, u_{myyy}$.

As with the original second-order scheme, to obtain the first-order derivatives of conservative variables, we need to update Eq. (9) to obtain the new values of conservative variables at the center. Now, for the fourth-order scheme, to update Eq. (9), we also need the new second-order derivatives of conservative variables at the center of the top face. To obtain the new second-order derivatives, we need the new third-order derivative. Therefore, the sequence to update the conservative variables in a complete half time step is as follows:

1: updating the third-order derivatives;
2: updating the second-order derivatives;
3: updating the conservative variables at the center;
4: updating the first-order derivatives.

Below, we describe the method to update the derivatives in the above sequence, which we mainly refer the thoughts of Shen et al. [14]. Some details we will describe more clearly according to our program debugging process. Here, we take the first half time step as an example.

3.1. Time-marching for the third-order derivatives of conservative variables

At the first half time step, we update the values at $C_i (i = 1, \cdots, 4)$. Below, we take C_1 as an example.

As in Fig. 2, at each of the points V_1, V_2, V_3, V_4 and its two neighbor points, by using the first-order Taylor expansion to approximate the second-order derivatives, we can obtain the third-order derivatives. Take points V_1 and u_{mxx} as an example.

u_{mxx} at the two neighbor points V_2 and V_4 of V_1 can be approximated by the first-order Taylor expansion from point V_1 as follows:

$$\begin{aligned} u_{mxx}(V_2') &= u_{mxx}(V_1') + u_{mxxx}(V_1')\Delta x_{V_2V_1} + u_{mxxy}(V_1')\Delta y_{V_2V_1}, \\ u_{mxx}(V_4') &= u_{mxx}(V_1') + u_{mxxx}(V_1')\Delta x_{V_4V_1} + u_{mxxy}(V_1')\Delta y_{V_4V_1}, \end{aligned} \tag{20}$$

where $\Delta x_{V_2V_1} = x_{V_2} - x_{V_1}$, $\Delta y_{V_2V_1} = y_{V_2} - y_{V_1}$, $\Delta x_{V_4V_1} = x_{V_4} - x_{V_1}$, $\Delta y_{V_4V_1} = y_{V_4} - y_{V_1}$.

$u_{mxx}(V_2')$ and $u_{mxx}(V_4')$ are the values at the new time step, and they can be evaluated using the values at the preceding half time level:

$$\begin{aligned} u_{mxx}(V_2') &= u_{mxx}(V_2) + u_{mxxt}(V_2)\frac{\Delta t}{2}, \\ u_{mxx}(V_4') &= u_{mxx}(V_4) + u_{mxxt}(V_4)\frac{\Delta t}{2}. \end{aligned} \tag{21}$$

By substituting Eq. (21) into Eq. (20) and then using Cramer's rule, we can obtain $u_{mxxx}(V_1')$ and $u_{mxxy}(V_1')$. For a fourth-order scheme, all the third-order derivatives are constants in every SE. Therefore,

$$u_{mxxx}(C_1') = u_{mxxx}(V_1'), u_{mxxy}(C_1') = u_{mxxy}(V_1'). \tag{22}$$

This way, we have obtained one group of $u_{mxxx}(C_1')$ and $u_{mxxy}(C_1')$.

Similarly, we can obtained another three groups of $u_{mxxx}(C_1')$ and $u_{mxxy}(C_1')$ from points V_2, V_3, V_4. Then, by directly using the arithmetic average or by using a weighted average function for a problem with discontinuities, the final values of $u_{mxxx}(C_1')$ and $u_{mxxy}(C_1')$ can be obtained. With the same strategy, by using u_{mxy}, u_{myx}, and u_{myy}, we can obtain the corresponding third-order derivatives (u_{mxyx}, u_{mxyy}), (u_{myxx}, u_{myxy}), and (u_{myyx}, u_{myyy}).

3.2. Time-marching for the second-order derivatives of conservative variables

By using the second-order Taylor expansion to approximate the first-order derivatives, we can obtain the second-order derivatives.

Below we take point V_1 and u_{mx} as an example.

$$\begin{aligned} u_{mx}(V_2') = {} & u_{mx}(V_1') + u_{mxx}(V_1')\Delta x_{V_2V_1} + u_{mxy}(V_1')\Delta y_{V_2V_1} + \frac{1}{2}\big[u_{mxxx}(V_1')(\Delta x_{V_2V_1})^2 \\ & + u_{mxxy}(V_1')\Delta x_{V_2V_1}\Delta y_{V_2V_1} + u_{mxyx}(V_1')\Delta x_{V_2V_1}\Delta y_{V_2V_1} + u_{mxyy}(V_1')(\Delta y_{V_2V_1})^2\big]. \end{aligned} \tag{23}$$

$$\begin{aligned} u_{mx}(V_4') = {} & u_{mx}(V_1') + u_{mxx}(V_1')\Delta x_{V_4V_1} + u_{mxy}(V_1')\Delta y_{V_4V_1} + \frac{1}{2}\big[u_{mxxx}(V_1')(\Delta x_{V_4V_1})^2 \\ & + u_{mxxy}(V_1')\Delta x_{V_4V_1}\Delta y_{V_4V_1} + u_{mxyx}(V_1')\Delta x_{V_4V_1}\Delta y_{V_4V_1} + u_{mxyy}(V_1')(\Delta y_{V_4V_1})^2\big]. \end{aligned} \tag{24}$$

In Eq. (23) and Eq. (24), the third-order derivatives were obtained in advance from section 3.1, and the first-order derivatives can be calculated from the preceding half time level; note that the Taylor expansion should include the second-order derivatives with respect to t. For example,

$$u_{mx}(V_2') = u_{mx}(V_2) + u_{mxt}(V_2)\frac{\Delta t}{2} + \frac{1}{2}u_{mxtt}(V_2)\left(\frac{\Delta t}{2}\right)^2.$$

By using Cramer's rule, we can obtain $u_{mxx}(V_1')$ and $u_{mxy}(V_1')$.

In contrast to the third-order derivatives, the second-order derivatives are not constants in every SE. Therefore, we must additionally use the first-order Taylor expansion to obtain the second-order derivatives at the center solution point. For example,

$$\begin{aligned} u_{mxx}(C_1') &= u_{mxx}(V_1') + u_{mxxx}(V_1')\Delta x_{C_1V_1} + u_{mxxy}(V_1')\Delta y_{C_1V_1}, \\ u_{mxy}(C_1') &= u_{mxy}(V_1') + u_{mxyx}(V_1')\Delta x_{C_1V_1} + u_{mxyy}(V_1')\Delta y_{C_1V_1}, \end{aligned} \tag{25}$$

where $\Delta x_{C_1V_1} = x_{C_1} - x_{V_1}$, $\Delta y_{C_1V_1} = y_{C_1} - y_{V_1}$.

Subsequently, treating like this at the points V_2, V_3, V_4, we can obtain four groups of $u_{mxx}(C_1')$ and $u_{mxy}(C_1')$, following which we finally obtain the new $u_{mxx}(C_1')$ and $u_{mxy}(C_1')$ by using the weighted average method.

By treating u_{my} with the same strategy, we can obtain the new $u_{myx}(C_1')$ and $u_{myy}(C_1')$.

After obtaining the third- and second-order derivatives, we can use Eq. (9) to obtain the new conservative variables $u_m(C_1')$.

3.3. Time-marching for the first-order derivatives of conservative variables

In contrast to the second- and third-order derivatives, the first-order derivatives are obtained from the values of conservative variables at points V_1, V_2, V_3, V_4 approximated by the third-order Taylor expansion from the center point C_1. For example,

$$\begin{aligned} u_m(V_k') = {} & u_m(C_1') + u_{mx}(C_1')\Delta x_{kC_1} + u_{my}(C_1')\Delta y_{kC_1} \\ & + \frac{1}{2}\big[u_{mxx}(C_1')(\Delta x_{kC_1})^2 + u_{myy}(C_1')(\Delta y_{kC_1})^2 \\ & + u_{mxy}(C_1')\Delta x_{kC_1}\Delta y_{kC_1} + u_{myx}(C_1')\Delta x_{kC_1}\Delta y_{kC_1}\big] \\ & + \frac{1}{6}\big[u_{mxxx}(C_1')(\Delta x_{kC_1})^3 + u_{mxxy}(C_1')(\Delta x_{kC_1})^2\Delta y_{kC_1} \\ & + u_{mxyx}(C_1')(\Delta x_{kC_1})^2\Delta y_{kC_1} + u_{mxyy}(C_1')(\Delta y_{kC_1})^2\Delta x_{kC_1} \\ & + u_{myxx}(C_1')(\Delta x_{kC_1})^2\Delta y_{kC_1} + u_{myxy}(C_1')(\Delta y_{kC_1})^2\Delta x_{kC_1} \\ & + u_{myyx}(C_1')(\Delta y_{kC_1})^2\Delta x_{kC_1} + u_{myyy}(C_1')(\Delta y_{kC_1})^3\big], \end{aligned} \tag{26}$$

where $\Delta x_{kC_1} = x_{V_k} - x_{C_1}$, $\Delta y_{kC_1} = y_{V_k} - y_{C_1}$, $k = 1, 2, 3, 4$.

In Eq. (26), the conservative variable $u_m(C_1')$ as well as its second- and third-order derivatives have all been calculated in advance, and $u_m(V_k')$ can be evaluated from the preceding half time level. For example,

$$u_m(V_k') = u_m(V_k) + u_{mt}(V_k)\frac{\Delta t}{2} + \frac{1}{2}u_{mtt}(V_k)\left(\frac{\Delta t}{2}\right)^2 + \frac{1}{6}u_{mttt}(V_k)\left(\frac{\Delta t}{2}\right)^3.$$

The conservative variable is then split into four groups according to (V_1, V_2), (V_2, V_3), (V_3, V_4), (V_4, V_1). By using Cramer's rule, we can get four groups of $u_{mx}(C_1')$ and $u_{my}(C_1')$. Then, the weighted average is used to obtain the final $u_{mx}(C_1')$ and $u_{my}(C_1')$.

As shown in Ref. [10] and [11], the weighted average function is defined as follows:

$$u_{mx}(C_1') = \begin{cases} 0 & \text{if } \theta_{mk} = 0 \\ \sum_{k=1}^{4}[(W_m^{(k)})^{\alpha} u_{mx}^{(k)}(C_1')]/(\sum_{k=1}^{4}(W_m^{(k)})^{\alpha} + \varepsilon) & \text{otherwise} \end{cases},$$

$$u_{my}(C_1') = \begin{cases} 0 & \text{if } \theta_{mk} = 0 \\ \sum_{k=1}^{4}[(W_m^{(k)})^{\alpha} u_{my}^{(k)}(C_1')]/(\sum_{k=1}^{4}(W_m^{(k)})^{\alpha} + \varepsilon) & \text{otherwise} \end{cases},$$

where

$$\theta_{mk} = \sqrt{[u_{mx}(C_1')]^2 + [u_{my}(C_1')]^2}, \qquad W_m^{(k)} = \prod_{j=1, j\neq k}^{4} \theta_{mk}, \quad m = 1, 2, \cdots, 8, k = 1, 2, 3, 4.$$

$\alpha \geq 0$ is an adjustable parameter that can control the viscosity of the scheme, and it is usually $\alpha = 0, 1, 2$. $\alpha = 1$ or 2 can reduce numerical oscillation in a strong discontinuity domain. ε is an infinitesimal. We use $\alpha = 2$ and $\varepsilon = 10^{-30}$.

In a similar manner, we can update the values of u_m and its derivatives at points C_2', C_3', C_4'. Then in the second half time step, by using the values at points C_1', C_2', C_3', C_4', the values at the final solution point G'' can be obtained.

4. New method for keeping the magnetic field divergence-free

In the process of obtaining a group of first-order derivatives in section 3.3, the number of equations is greater than the number of unknowns. This overdetermined equations inspires the use of the least-squares method to obtain the final solutions.

The magnetic field divergence-free condition is as follows:

$$\nabla \cdot \boldsymbol{B} = \frac{\partial B_x}{\partial x} + \frac{\partial B_y}{\partial y} = u_{6x} + u_{7y} = 0. \tag{27}$$

When using the least-squares method to solve the first-order derivatives relative to B_x, B_y, Eq. (27) can be combined with other equations relative to B_x and B_y to obtain a new overdetermined equations. Thus, by using the least-squares method, the magnetic field divergence can be fundamentally controlled.

The basic concept of the least-squares method is as follows:

For an overdetermined equations expressed in the matrix form as:

$$AX = C, \tag{28}$$

where

$$A = \begin{bmatrix} a_{11} & a_{12} & \ldots & a_{1j} \\ a_{21} & a_{22} & \ldots & a_{2j} \\ \cdot & \cdot & \cdot & \cdot \\ \cdot & \cdot & \cdot & \cdot \\ a_{i1} & a_{i2} & \ldots & a_{ij} \end{bmatrix} = [L_1, L_2, \ldots, L_j], \qquad X = \begin{bmatrix} x_1 \\ x_2 \\ \cdot \\ \cdot \\ x_j \end{bmatrix}, \qquad C = \begin{bmatrix} c_1 \\ c_2 \\ \cdot \\ \cdot \\ c_i \end{bmatrix}, \quad i > j,$$

According to a mathematic theorem (Theorem 5.1 of [32]), $A^{\mathrm{T}}AX = A^{\mathrm{T}}C$ is the normal equations for an overdetermined equations. The solution of the normal equations is also the least-squares solution of the overdetermined equations.

$$\begin{bmatrix} l_{11} & l_{12} & \cdot & \cdot & l_{1j} \\ l_{21} & l_{22} & \cdot & \cdot & l_{2j} \\ \cdot & \cdot & \cdot & \cdot & \cdot \\ \cdot & \cdot & \cdot & \cdot & \cdot \\ l_{j1} & l_{j2} & \cdot & \cdot & l_{jj} \end{bmatrix} \begin{bmatrix} x_1 \\ x_2 \\ \cdot \\ \cdot \\ x_j \end{bmatrix} = \begin{bmatrix} L_1^{\mathrm{T}} \bullet C \\ L_2^{\mathrm{T}} \bullet C \\ \cdot \\ \cdot \\ L_j^{\mathrm{T}} \bullet C \end{bmatrix}, \tag{29}$$

where $l_{mn} = L_m^{\mathrm{T}} \bullet L_n$ $(m, n = 1, 2, \cdots, j)$.

For the normal equations expressed by Eq. (29), we need to use a matrix solver method, such as QR factorization or multiplication with the pseudo-inverse of A. We use the Lapack function gesvx(a, b, x) to solve it.

When using the least-squares method to solve the first-order derivatives relative to B_x, B_y, all the equations are expressed in the matrix form as follows:

$$A=\begin{bmatrix} \Delta x_{1C_1} & \Delta y_{1C_1} & 0 & 0 \\ \Delta x_{2C_1} & \Delta y_{2C_1} & 0 & 0 \\ \Delta x_{3C_1} & \Delta y_{3C_1} & 0 & 0 \\ \Delta x_{4C_1} & \Delta y_{4C_1} & 0 & 0 \\ 0 & 0 & \Delta x_{1C_1} & \Delta y_{1C_1} \\ 0 & 0 & \Delta x_{2C_1} & \Delta y_{2C_1} \\ 0 & 0 & \Delta x_{3C_1} & \Delta y_{3C_1} \\ 0 & 0 & \Delta x_{4C_1} & \Delta y_{4C_1} \\ 1 & 0 & 0 & 1 \end{bmatrix}, \qquad X=[u_{6x}, u_{6y}, u_{7x}, u_{7y}]^{\mathrm{T}},$$

$$\begin{aligned} \mathrm{C}(1) &= u_6(\mathrm{V}_1') - u_6(\mathrm{C}_1') \\ &\quad - \frac{1}{2}\big[u_{6xx}(\mathrm{C}_1')(\Delta x_{1C_1})^2 + \mathrm{u}_{6xy}(\mathrm{C}_1')\Delta \mathrm{x}_{1C_1}\Delta y_{1C_1} \\ &\quad + u_{6yx}(\mathrm{C}_1')\Delta \mathrm{x}_{1C_1}\Delta \mathrm{y}_{1C_1} + u_{6yy}(\mathrm{C}_1')(\Delta \mathrm{y}_{1C_1})^2\big] \\ &\quad - \frac{1}{6}\big[u_{6xxx}(\mathrm{C}_1')(\Delta \mathrm{x}_{1C_1})^3 + u_{6xxy}(\mathrm{C}_1')(\Delta \mathrm{x}_{1C_1})^2\Delta \mathrm{y}_{1C_1} \\ &\quad + u_{6xyx}(\mathrm{C}_1')(\Delta \mathrm{x}_{1C_1})^2\Delta \mathrm{y}_{1C_1} + u_{6xyy}(\mathrm{C}_1')(\Delta \mathrm{y}_{1C_1})^2\Delta \mathrm{x}_{1C_1} \\ &\quad + u_{6yxx}(\mathrm{C}_1')(\Delta \mathrm{x}_{1C_1})^2\Delta \mathrm{y}_{1C_1} + u_{6yxy}(\mathrm{C}_1')(\Delta \mathrm{y}_{1C_1})^2\Delta \mathrm{x}_{1C_1} \\ &\quad + u_{6yyx}(\mathrm{C}_1')(\Delta \mathrm{y}_{1C_1})^2\Delta \mathrm{x}_{1C_1} + u_{6yyy}(\mathrm{C}_1')(\Delta \mathrm{y}_{1C_1})^3\big], \end{aligned}$$

$$\begin{aligned} \mathrm{C}(2) &= u_6(\mathrm{V}_2') - u_6(\mathrm{C}_1') \\ &\quad - \frac{1}{2}\big[u_{6xx}(\mathrm{C}_1')(\Delta x_{2C_1})^2 + u_{6xy}(\mathrm{C}_1')\Delta x_{2C_1}\Delta y_{2C_1} \\ &\quad + u_{6yx}(\mathrm{C}_1')\Delta x_{2C_1}\Delta y_{2C_1} + u_{6yy}(\mathrm{C}_1')(\Delta y_{2C_1})^2\big] \\ &\quad - \frac{1}{6}\big[u_{6xxx}(\mathrm{C}_1')(\Delta x_{2C_1})^3 + u_{6xxy}(\mathrm{C}_1')(\Delta x_{2C_1})^2\Delta y_{2C_1} \\ &\quad + u_{6xyx}(\mathrm{C}_1')(\Delta x_{2C_1})^2\Delta y_{2C_1} + u_{6xyy}(\mathrm{C}_1')(\Delta y_{2C_1})^2\Delta x_{2C_1} \\ &\quad + u_{6yxx}(\mathrm{C}_1')(\Delta x_{2C_1})^2\Delta y_{2C_1} + u_{6yxy}(\mathrm{C}_1')(\Delta y_{2C_1})^2\Delta x_{2C_1} \\ &\quad + u_{6yyx}(\mathrm{C}_1')(\Delta y_{2C_1})^2\Delta x_{2C_1} + u_{6yyy}(\mathrm{C}_1')(\Delta y_{2C_1})^3\big], \end{aligned}$$

$$\begin{aligned} \mathrm{C}(3) &= u_6(\mathrm{V}_3') - u_6(\mathrm{C}_1') \\ &\quad - \frac{1}{2}\big[u_{6xx}(\mathrm{C}_1')(\Delta x_{3C_1})^2 + u_{6xy}(\mathrm{C}_1')\Delta x_{3C_1}\Delta y_{3C_1} \\ &\quad + u_{6yx}(\mathrm{C}_1')\Delta x_{3C_1}\Delta y_{3C_1} + u_{6yy}(\mathrm{C}_1')(\Delta y_{3C_1})^2\big] \\ &\quad - \frac{1}{6}\big[u_{6xxx}(\mathrm{C}_1')(\Delta x_{3C_1})^3 + u_{6xxy}(\mathrm{C}_1')(\Delta x_{3C_1})^2\Delta y_{3C_1} \\ &\quad + u_{6xyx}(\mathrm{C}_1')(\Delta x_{3C_1})^2\Delta y_{3C_1} + u_{6xyy}(\mathrm{C}_1')(\Delta y_{3C_1})^2\Delta x_{3C_1} \\ &\quad + u_{6yxx}(\mathrm{C}_1')(\Delta x_{3C_1})^2\Delta y_{3C_1} + u_{6yxy}(\mathrm{C}_1')(\Delta y_{3C_1})^2\Delta x_{3C_1} \\ &\quad + u_{6yyx}(\mathrm{C}_1')(\Delta y_{3C_1})^2\Delta x_{3C_1} + u_{6yyy}(\mathrm{C}_1')(\Delta y_{3C_1})^3\big], \end{aligned}$$

$$\begin{aligned} \mathrm{C}(4) &= u_6(\mathrm{V}_4') - u_6(\mathrm{C}_1') \\ &\quad - \frac{1}{2}\big[u_{6xx}(\mathrm{C}_1')(\Delta x_{4C_1})^2 + u_{6xy}(\mathrm{C}_1')\Delta x_{4C_1}\Delta y_{4C_1} \\ &\quad + u_{6yx}(\mathrm{C}_1')\Delta x_{4C_1}\Delta y_{4C_1} + u_{6yy}(\mathrm{C}_1')(\Delta y_{4C_1})^2\big] \\ &\quad - \frac{1}{6}\big[u_{6xxx}(\mathrm{C}_1')(\Delta x_{4C_1})^3 + u_{6xxy}(\mathrm{C}_1')(\Delta x_{4C_1})^2\Delta y_{4C_1} \\ &\quad + u_{6xyx}(\mathrm{C}_1')(\Delta x_{4C_1})^2\Delta y_{4C_1} + u_{6xyy}(\mathrm{C}_1')(\Delta y_{4C_1})^2\Delta x_{4C_1} \\ &\quad + u_{6yxx}(\mathrm{C}_1')(\Delta x_{4C_1})^2\Delta y_{4C_1} + u_{6yxy}(\mathrm{C}_1')(\Delta y_{4C_1})^2\Delta x_{4C_1} \\ &\quad + u_{6yyx}(\mathrm{C}_1')(\Delta y_{4C_1})^2\Delta x_{4C_1} + u_{6yyy}(\mathrm{C}_1')(\Delta y_{4C_1})^3\big], \end{aligned}$$

$$
\begin{aligned}
C(5) &= u_7(V_1') - u_7(C_1') \\
&\quad - \frac{1}{2}\big[u_{7xx}(C_1')(\Delta x_{1C_1})^2 + u_{7xy}(C_1')\Delta x_{1C_1}\Delta y_{1C_1} \\
&\quad + u_{7yx}(C_1')\Delta x_{1C_1}\Delta y_{1C_1} + u_{7yy}(C_1')(\Delta y_{1C_1})^2\big] \\
&\quad - \frac{1}{6}\big[u_{7xxx}(C_1')(\Delta x_{1C_1})^3 + u_{7xxy}(C_1')(\Delta x_{1C_1})^2\Delta y_{1C_1} \\
&\quad + u_{7xyx}(C_1')(\Delta x_{1C_1})^2\Delta y_{1C_1} + u_{7xyy}(C_1')(\Delta y_{1C_1})^2\Delta x_{1C_1} \\
&\quad + u_{7yxx}(C_1')(\Delta x_{1C_1})^2\Delta y_{1C_1} + u_{7yxy}(C_1')(\Delta y_{1C_1})^2\Delta x_{1C_1} \\
&\quad + u_{7yyx}(C_1')(\Delta y_{1C_1})^2\Delta x_{1C_1} + u_{7yyy}(C_1')(\Delta y_{1C_1})^3\big], \\
C(6) &= u_7(V_2') - u_7(C_1') \\
&\quad - \frac{1}{2}\big[u_{7xx}(C_1')(\Delta x_{2C_1})^2 + u_{7xy}(C_1')\Delta x_{2C_1}\Delta y_{2C_1} \\
&\quad + u_{7yx}(C_1')\Delta x_{2C_1}\Delta y_{2C_1} + u_{7yy}(C_1')(\Delta y_{2C_1})^2\big] \\
&\quad - \frac{1}{6}\big[u_{7xxx}(C_1')(\Delta x_{2C_1})^3 + u_{7xxy}(C_1')(\Delta x_{2C_1})^2\Delta y_{2C_1} \\
&\quad + u_{7xyx}(C_1')(\Delta x_{2C_1})^2\Delta y_{2C_1} + u_{7xyy}(C_1')(\Delta y_{2C_1})^2\Delta x_{2C_1} \\
&\quad + u_{7yxx}(C_1')(\Delta x_{2C_1})^2\Delta y_{2C_1} + u_{7yxy}(C_1')(\Delta y_{2C_1})^2\Delta x_{2C_1} \\
&\quad + u_{7yyx}(C_1')(\Delta y_{2C_1})^2\Delta x_{2C_1} + u_{7yyy}(C_1')(\Delta y_{2C_1})^3\big], \\
C(7) &= u_7(V_3') - u_7(C_1') \\
&\quad - \frac{1}{2}\big[u_{7xx}(C_1')(\Delta x_{3C_1})^2 + u_{7xy}(C_1')\Delta x_{3C_1}\Delta y_{3C_1} \\
&\quad + u_{7yx}(C_1')\Delta x_{3C_1}\Delta y_{3C_1} + u_{7yy}(C_1')(\Delta y_{3C_1})^2\big] \\
&\quad - \frac{1}{6}\big[u_{7xxx}(C_1')(\Delta x_{3C_1})^3 + u_{7xxy}(C_1')(\Delta x_{3C_1})^2\Delta y_{3C_1} \\
&\quad + u_{7xyx}(C_1')(\Delta x_{3C_1})^2\Delta y_{3C_1} + u_{7xyy}(C_1')(\Delta y_{3C_1})^2\Delta x_{3C_1} \\
&\quad + u_{7yxx}(C_1')(\Delta x_{3C_1})^2\Delta y_{3C_1} + u_{7yxy}(C_1')(\Delta y_{3C_1})^2\Delta x_{3C_1} \\
&\quad + u_{7yyx}(C_1')(\Delta y_{3C_1})^2\Delta x_{3C_1} + u_{7yyy}(C_1')(\Delta y_{3C_1})^3\big], \\
C(8) &= u_7(V_4') - u_7(C_1') \\
&\quad - \frac{1}{2}\big[u_{7xx}(C_1')(\Delta x_{4C_1})^2 + u_{7xy}(C_1')\Delta x_{4C_1}\Delta y_{4C_1} \\
&\quad + u_{7yx}(C_1')\Delta x_{4C_1}\Delta y_{4C_1} + u_{7yy}(C_1')(\Delta y_{4C_1})^2\big] \\
&\quad - \frac{1}{6}\big[u_{7xxx}(C_1')(\Delta x_{4C_1})^3 + u_{7xxy}(C_1')(\Delta x_{4C_1})^2\Delta y_{4C_1} \\
&\quad + u_{7xyx}(C_1')(\Delta x_{4C_1})^2\Delta y_{4C_1} + u_{7xyy}(C_1')(\Delta y_{4C_1})^2\Delta x_{4C_1} \\
&\quad + u_{7yxx}(C_1')(\Delta x_{4C_1})^2\Delta y_{4C_1} + u_{7yxy}(C_1')(\Delta y_{4C_1})^2\Delta x_{4C_1} \\
&\quad + u_{7yyx}(C_1')(\Delta y_{4C_1})^2\Delta x_{4C_1} + u_{7yyy}(C_1')(\Delta y_{4C_1})^3\big], \\
C(9) &= 0,
\end{aligned}
$$

where

$$
\Delta x_{1C_1} = x_{V_1} - x_{C_1}, \quad \Delta x_{2C_1} = x_{V_2} - x_{C_1}, \quad \Delta x_{3C_1} = x_{V_3} - x_{C_1}, \quad \Delta x_{4C_1} = x_{V_4} - x_{C_1},
$$

$$
\Delta y_{1C_1} = y_{V_1} - y_{C_1}, \quad \Delta y_{2C_1} = y_{V_2} - y_{C_1}, \quad \Delta y_{3C_1} = y_{V_3} - y_{C_1}, \quad \Delta y_{4C_1} = y_{V_4} - y_{C_1}.
$$

By using this method, we can obtain $u_{6x}, u_{6y}, u_{7x}, u_{7y}$. The other first-order derivatives are still obtained using the method presented in section 3.3.

5. Numerical tests

In this section, we use some benchmarks to test the validity of our proposed method. We first test the accuracy of our scheme. Then, by comparing the average magnetic field divergence error and some magnetic field divergence distribution

Table 1
Numerical error and error convergence rate.

N	v_x		v_y		v_z		p	
	error	order	error	order	error	order	error	order
32	5.031E−06		5.031E−06		7.115E−06		1.380E−06	
64	2.058E−07	4.6115	2.058E−07	4.6115	2.911E−07	4.6113	5.210E−08	4.7272
128	9.745E−09	4.4004	9.745E−09	4.4004	1.378E−08	4.4009	2.170E−09	4.5855
256	5.252E−10	4.2137	5.252E−10	4.2137	7.428E−10	4.2135	1.015E−10	4.4181

B_x		B_y		B_z		average		div$B$	
error	order	error	order	error	order	error	order	error	order
5.031E−06		5.031E−06		7.115E−06		7.115E−06		3.122E−16	
2.058E−07	4.6115	2.058E−07	4.6115	2.911E−07	4.6113	2.911E−07	4.6113	1.178E−17	4.7281
9.745E−09	4.4004	9.745E−09	4.4004	1.378E−08	4.4009	1.378E−08	4.4009	4.913E−19	4.5836
5.252E−10	4.2137	5.252E−10	4.2137	7.428E−10	4.2135	7.428E−10	4.2135	2.296E−20	4.4194

contour plots, we demonstrate the excellent characteristics of the new method for keeping the magnetic field divergence-free.

The average magnetic field divergence error is defined as follows [15]:

$$\text{div}B\_\text{average\_error} = \frac{\sum_{i=1}^{\text{M}} |(\nabla \cdot \boldsymbol{B})_i|}{\text{M}}, \tag{30}$$

where $(\nabla \cdot \boldsymbol{B})_i$ is the magnetic divergence in the i-th computed grid point and M is the total number of computed grid points with one time step.

5.1. Smooth Alfvén wave problem

The smooth Alfvén wave problem [17] is a very good example to test the accuracy of the scheme [33,34], and it was first proposed by Gabor Tóth. Here, we use the smooth Alfvén wave problem to test the accuracy of our scheme.

This problem concerns the evolution of a circularly polarized Alfvén wave with a periodic boundary condition. Its initial conditions are given as:

$$\rho = 1, \qquad v_{//} = 0, \qquad v_{\perp} = 0.1\sin(2\pi x_1), \qquad v_z = 0.1\cos(2\pi x_1),$$
$$p = 0.1, \qquad B_{//} = 1, \qquad B_{\perp} = v_{\perp}, \qquad B_z = v_z,$$

where $x_1 = x\cos(\theta) + y\sin(\theta)$ and θ is the Alfvén wave propagation angle with respect to the x-axis. In this paper, we utilize $\theta = \frac{\pi}{4}$. Other values can also be used; for example, Ref. [17] used $\theta = \frac{\pi}{6}$, and Ref. [34] used $\theta = \arctan(2)$. The calculation domain is $[0, 1/\cos\theta] \times [0, 1/\sin\theta]$.

The relationships between $v_{//}, v_{\perp}$ and v_x, v_y, $B_{//}, B_{\perp}$ and B_x, B_y are:

$$\zeta_{//} = \zeta_x\cos(\theta) + \zeta_y\sin(\theta),$$
$$\zeta_{\perp} = -\zeta_x\sin(\theta) + \zeta_y\cos(\theta), \quad (\zeta = v \text{ or } B).$$

Under these initial conditions, the Alfvén wave propagates periodically with a constant wavelength $\lambda = 1$; when the time t becomes an integer, it returns to the initial state. Therefore, the initial values are also the exact solution. As Tóth [17] suggests, we use $0.4/N$ with an $N \times N$ uniform grid as the time step so that the system can reach an integer time t.

In Table 1, we list the numerical error of some primitive variables and average magnetic field divergence as well as the average error and the relative error convergence rate at $t = 2$. Tóth [17] stated that the density does not participate in the Alfvén wave and that its errors are negligible. Therefore, we do not consider the density. The average error is defined by

$$L_N(\text{average}) = \frac{1}{4}\big[L_N(v_{\perp}) + L_N(v_z) + L_N(B_{\perp}) + L_N(B_z)\big], \tag{31}$$

where L_N represents the numerical error.

The numerical error is defined as follows:

$$L_N(u_m) = \frac{\sum_{i=1}^{\text{M}} |(u_m)_i^{num} - (u_m)_i^{exact}|}{\text{M}}. \tag{32}$$

where The superscript "*num*" represents numerical solution and "*exact*" denotes exact solution. M is the total number of calculated grid points with one time step.

Then, the error convergence rate (accuracy order) is computed as:

$$\text{order} = \log(L_{N_1}/L_{N_2})/\log(N_2/N_1). \tag{33}$$

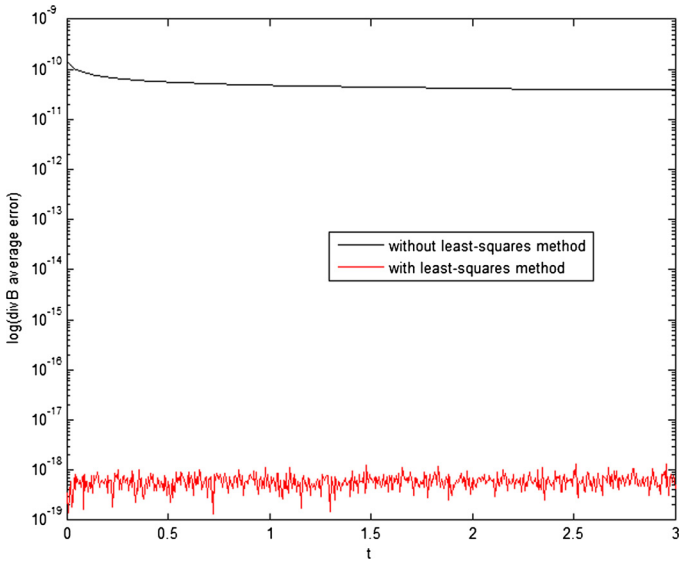

Fig. 3. Average magnetic field divergence error with 128×128 grids for the smooth Alfvén wave problem. The horizontal axis represents time.

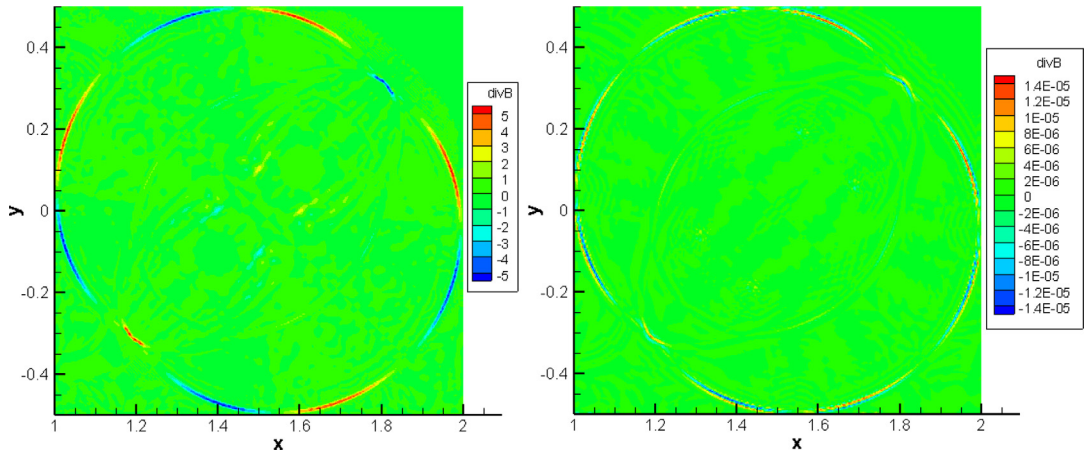

(a) $t = 0.2$, using only the original fourth-order scheme

(b) $t = 0.2$, using the fourth-order scheme with the new divergence-free method

Fig. 4. Distribution of the magnetic field divergence error with 256×256 grids for the MHD blast wave problem at $t = 0.2$.

5.2. MHD vortex problem

The MHD vortex problem, also called the Orszag–Tang MHD turbulence problem, was first proposed by Orszag et al. in 1979. It is often used to test 2D MHD codes [17,28,35]. It includes some important characteristics of MHD turbulence in which some shocks and other discontinuities occur as time evolves. The initial values are expressed as follows:

$$\rho = \gamma^2, \qquad p = \gamma,$$
$$v_x = -\sin(y), \qquad v_y = \sin(x), \qquad v_z = 0,$$
$$B_x = -\sin(y), \qquad B_y = \sin(2x), \qquad B_z = 0.$$

where $\gamma = \frac{5}{3}$. The calculation domain is $[0, 2\pi] \times [0, 2\pi]$, and a periodic boundary is used.

5.3. MHD blast wave problem

The MHD blast problem is initiated by an over-pressured region in the center of a strongly magnetized medium with low plasma β [28]. The region drives fast shocks moving outward, compressing the plasma and magnetic field ahead and leaving rarefied plasma behind.

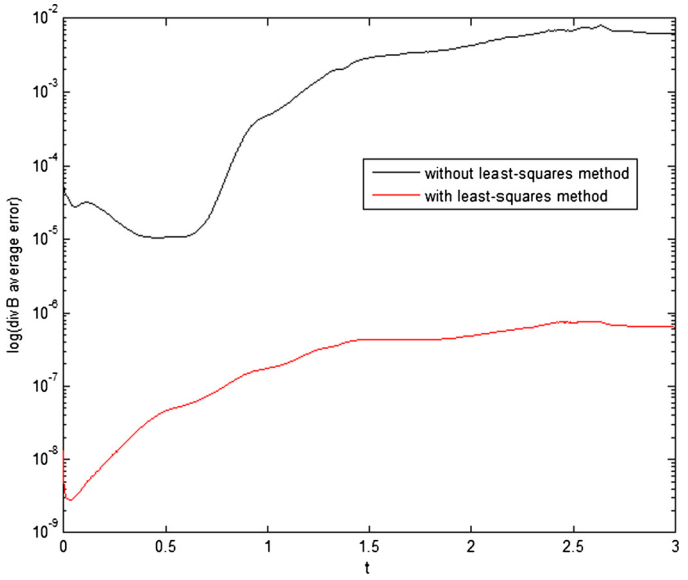

Fig. 5. Average magnetic field divergence error with 256×256 grids for the MHD vortex problem. The horizontal axis represents time.

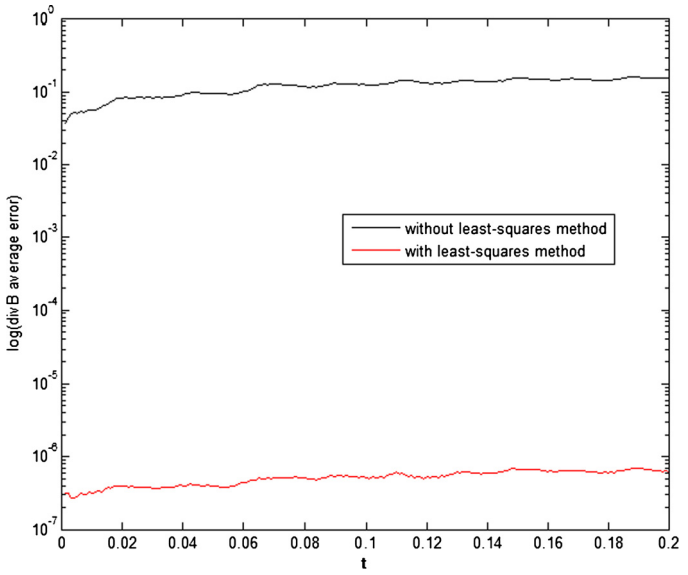

Fig. 6. Average magnetic field divergence error with 256×256 grids for the MHD blast wave problem. The horizontal axis represents time.

The calculation domain is $[1, 2] \times [-0.5, 0.5]$, and a fixed boundary is used. The initial conditions are expressed as follows:

$$\rho = 1, \qquad v_x = v_y = v_z = 0, \qquad B_x = B_y = 1/\sqrt{2}, \qquad B_z = 0,$$

$$p = \begin{cases} 10 & \text{if } \sqrt{(x-1.5)^2 + y^2} < 0.1 \\ 0.1 & \text{otherwise} \end{cases}.$$

The relative test results are as follows:

Fig. 3, Fig. 5, and Fig. 6 compare the evolution of the average magnetic-field divergence error with time between the original fourth-order schemes with and without the least-squares method for attaining $\mathrm{div} B = 0$. Fig. 4 and Fig. 7 show contour plots of the magnetic-field divergence distribution for these two cases. From these figures, we clearly observe that the use of the least-squares method can control the magnetic divergence efficiently, and the order of magnetic divergence error can be reduced to approximately 5∼8. Fig. 8 and Fig. 9 give the contour plots of pressure for MHD vortex problem at $t = 3$ and MHD blast wave problem at $t = 0.2$, respectively. We can see the structures are much clearer and identified by using the fourth-order CESE scheme (the right column) than the second-order CESE scheme (the left column). To compare

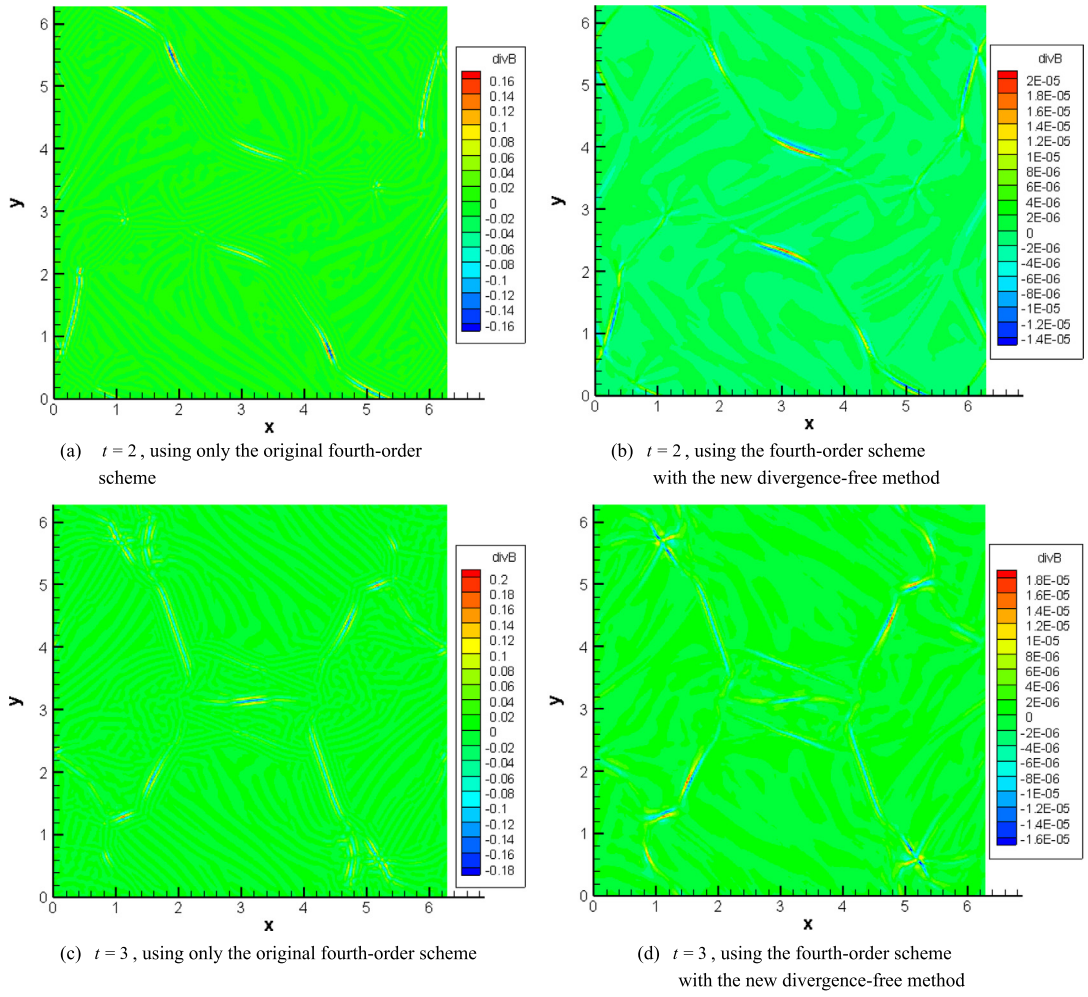

(a) $t = 2$, using only the original fourth-order scheme

(b) $t = 2$, using the fourth-order scheme with the new divergence-free method

(c) $t = 3$, using only the original fourth-order scheme

(d) $t = 3$, using the fourth-order scheme with the new divergence-free method

Fig. 7. Distribution of the magnetic-field divergence error with 256×256 grids for the MHD vortex problem at $t = 2$ (the first row) and $t = 3$ (the second row).

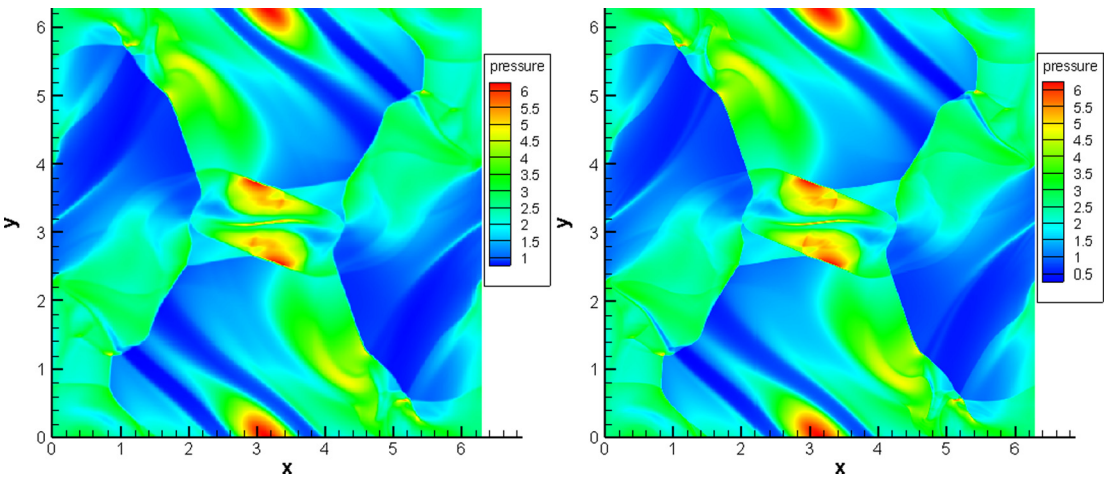

Fig. 8. The contour plots of pressure for MHD vortex problem at $t = 3$ with 512×512 grids by using second-order (the left column) and fourth-order (the right column) CESE scheme, respectively.

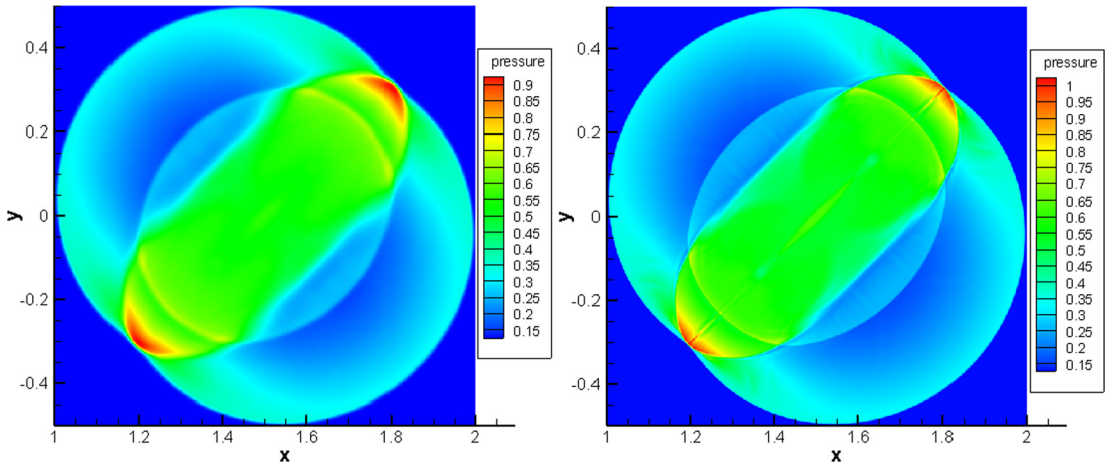

Fig. 9. The contour plots of pressure for MHD blast wave problem at $t = 0.2$ with 256×256 grids by using second-order (left column) and fourth-order (right column) CESE scheme, respectively.

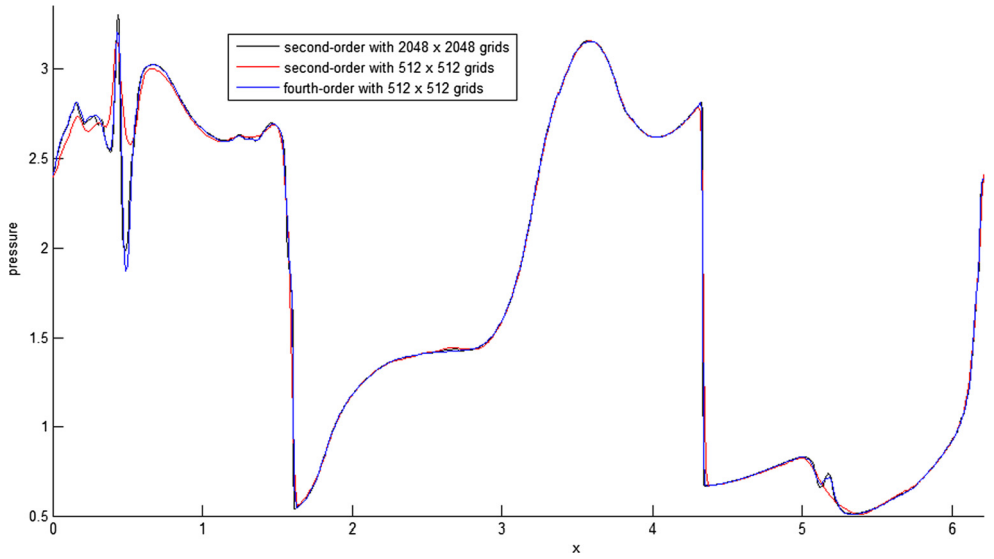

Fig. 10. The pressures along the line of $y = 0.625\pi$ at $t = 3$ for MHD vortex problem: the black line is using second-order scheme with 2048×2048 grids; the red line is using second-order scheme with 512×512 grids; the blue line is using fourth-order scheme with 512×512 grids. (For interpretation of the references to color in this figure legend, the reader is referred to the web version of this article.)

in details and more clearly, we also compare the pressures along the line of $y = 0.625\pi$ at $t = 3$ for MHD vortex problem (Fig. 10) and along line through the center of the blast wave at $t = 0.2$, namely $y = 0$ for blast wave problem (Fig. 11). As Fig. 10 and Fig. 11 show, the fourth-order CESE scheme (the blue lines) has remarkable advantages over the second-order CESE scheme (the red lines) in terms of accuracy at the same grid resolution. We also test the CPU time, we use the Intel Fortran compiler and run on the Intel Xeon E7450 with a CPU clock speed of 2.4 GHz, and using O4 optimization option. And we find the second-order scheme need about 379 seconds and the fourth-order need about 4068 seconds for vortex problem with 512×512 grids by using 24 processors. But from Fig. 10 and Fig. 11 we can see the fourth-order scheme with less grids can achieve the similar even much better result than the second-order scheme with more grids. What's more, the cost of second-order scheme with much more grids is much larger, such as the vortex problem with 2048×2048 grids, it need at least 60 processors, and the CPU time is about 4722 seconds. At this case, the fourth-order scheme with 512×512 grids only need CPU time 1556 seconds. Giving a comprehensive consideration about the computation accuracy and efficiency, the fourth-order is not expensive than the second-order scheme and can achieve a better result. Solving the induction equation only occupy very little parts of the total time, the mainly occupied time is the solving the fluxes. Here, we have optimized our code to reduce some unnecessary redundant calculations, such as the derivations with respect to time t of fluxes and conservative variables as the sequence given in section 3 will be economic and effective.

About the stability condition, it's mainly related to the CFL number, here, we have tried the CFL number from 0.3 to 0.8, they all can maintain a good running and hasn't produced negative pressure or negative density. For the MHD vortex and

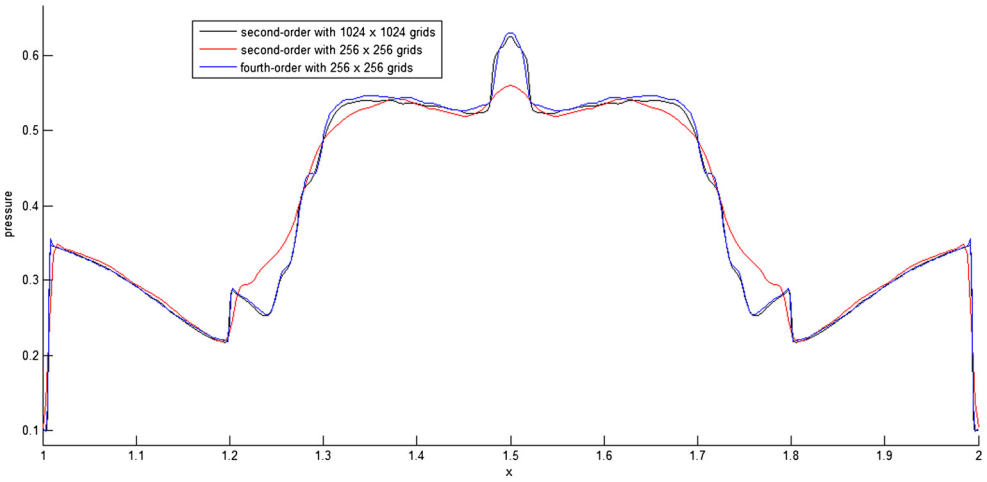

Fig. 11. The pressures along line through the center ($y = 0$) of the blast wave at $t = 0.2$ for MHD blast wave problem: the black line is using second-order scheme with 1024×1024 grids; the red line is using second-order scheme with 256×256 grids; the blue line is using fourth-order scheme with 256×256 grids. (For interpretation of the references to color in this figure legend, the reader is referred to the web version of this article.)

blast wave problems, both of them the CFL number used are 0.8, namely, this fourth-order scheme permit a larger time step [36] which can help to reduce the calculation cost.

6. Conclusions

For MHD simulation, this study is the first to extend the second-order CESE scheme to a high order successfully, and the tests demonstrate the feasibility of this scheme. This method has the following main advantages:

(1) It uses a compact stencil as in the second-order scheme and can be easily extended to arbitrary much higher order.

(2) The spatial and temporal discretization can simultaneously reach a significantly high order with one time step, which is difficult to achieve with FVM and FDM.

(3) By taking advantage of the merits of the CESE scheme, the use of the least-squares solution method can fundamentally control the magnetic field divergence error.

In future work, we aim to apply this new method to magnetic reconnection, solar wind, and interactions of solar wind with the earth's atmosphere to study these space physics problems more accurately using numerical simulation methods.

Acknowledgements

The work is jointly supported by the National Basic Research Program of China (Grant No. 2012CB825601), the National Natural Science Foundation of China (Grant Nos. 41231068, 41504132, 41274192, and 41531073), the Knowledge Innovation Program of the Chinese Academy of Sciences (Grant No. KZZD-EW-01-4), and the Specialized Research Fund for State Key Laboratories. The numerical calculation has been completed on our SIGMA Cluster computing system. The authors thank Dr. Hua Shen's inspiring discussions.

References

[1] X.Y. Wang, A Summary of the Space–Time Conservation Element and Solution Element (CESE), method, NASA/TM-2015-218743, 2015.
[2] L. Ivan, Development of High-Order CENO Finite-Volume Schemes with Block-Based Adaptive Mesh Refinement, PhD thesis, University of Toronto, October 2010.
[3] D.S. Balsara, C. Meyer, M. Dumbser, H.J. Du, Z.L. Xu, Efficient Implementation of ADER schemes for Euler and Magnetohydrodynamical flows on structured meshes-speed comparisons with Runge–Kutta methods, J. Comput. Phys. 235 (2013) 934–969.
[4] D.S. Balsara, T. Rumpf, M. Dumbser, C.D. Munz, Efficient, high accuracy ADER-WENO schemes for hydrodynamics and divergence-free magnetohydrodynamics, J. Comput. Phys. 228 (2009) 2480–2516.
[5] D.S. Balsara, Higher order accuracy space–time schemes for computational astrophysics—Part I—finite volume methods, 3, arXiv:1703.01241, 2017.
[6] H. Shen, C.Y. Wen, D.L. Zhang, A characteristic space–time conservation element and solution element method for conservation laws, J. Comput. Phys. 288 (2015) 101–118.
[7] Andrew J. Christlieb, Yaman Guclu, David C. Seal, The PICARD integral formulation of weighted essentially nonoscillatory schemes, SIAM J. Numer. Anal 53 (4) (2015) 1833–1856.
[8] S.T. Li, Higher-order time integration with a local Lax–Wendroff procedure for a central scheme on an overlapping grid, J. Comput. Appl. Math. 236 (2012) 4756–4761.
[9] S.C. Chang, The method of space–time conservation element and solution element—a new approach for solving the Navier–Stokes and Euler equations, J. Comput. Phys. 119 (1995) 295–324.
[10] S.C. Chang, A New Approach for Constructing Highly Stable High Order CESE Schemes, NASA/TM 2010-216766, 2010.

[11] D. Bilyeu, Y.Y. Chen, S.T. John Yu, High-order CESE methods for the Euler equations, in: 49th AIAA Aerospace Sciences Meeting Including the New Horizons Forum and Aerospace Exposition, Orlando, Florida, 4–7 Jan., 2011, AIAA 2011-298.
[12] D. Bilyeu, A High-Order Conservation Element Solution Element Method for Solving Hyperbolic Differential Equations on Unstructured Grid, PhD thesis, University of the Ohio State, 2014.
[13] K.X. Liu, J.T. Wang, Analysis of high accuracy conservation element and solution element schemes, Chin. Phys. Lett. 21 (2004) 2085–2088.
[14] H. Shen, C.Y. Wen, K.X. Liu, Robust high-order space–time conservative schemes for solving conservation on hybrid Meshes, J. Comput. Phys. 281 (2015) 375–402.
[15] X.S. Feng, Y.Q. Hu, F.S. Wei, Modeling the resistive MHD by the CESE method, Sol. Phys. 235 (2006) 235–257.
[16] R.L. Jiang, C. Fang, P.F. Chen, A new MHD code with adaptive mesh refinement and parallelization for astrophysics, Comput. Phys. Commun. 183 (2012) 1617–1633.
[17] G. Tóth, The constraint in shock-capturing magnetohydrodynamics codes, J. Comput. Phys. 161 (2000) 605–652.
[18] M. Zhang, X.S. Feng, A comparative study of divergence cleaning methods of magnetic field in the solar coronal numerical simulation, Front. Astron. Space Sci. 3 (2016) 6.
[19] K.G. Powell, P.L. Roe, T.J. Linde, T.I. Gombosi, D.L. DeZeeuw, A solution-adaptive upwind scheme for ideal magnetohydrodynamics, J. Comput. Phys. 154 (1999) 284–309.
[20] J.U. Brackbill, D.C. Barnes, The effect of nonzero $\nabla \cdot B$ on the numerical solution of the magnetohydrodynamic equations, J. Comput. Phys. 35 (1980) 426–430.
[21] B. vanderHolst, R. Keppens, Hybrid block-AMR in Cartesian and Curvilinear coordinates: MHD applications, J. Comput. Phys. 226 (2007) 925–946.
[22] C.R. Evans, J.F. Hawley, Simulation of magnetohydrodynamic flows—a constrained transport method, Astrophys. J. 332 (1988) 659–677.
[23] A. Dedner, F. Kemm, D. Kröner, C.D. Munz, T. Schnitzer, W. Wesenberg, Hyperbolic divergence cleaning for the MHD equations, J. Comput. Phys. 175 (2002) 645–673.
[24] D.S. Balsara, Second-order-accurate schemes for magnetohydrodynamics with divergence-free reconstruction, Astrophys. J. Suppl. Ser. 151 (2004) 149–184.
[25] D.S. Balsara, Divergence-free adaptive mesh refinement for Magnetohydrodynamics, J. Comput. Phys. 174 (2001) 614–648.
[26] D.S. Balsara, D.S. Spicer, A staggered mesh algorithm using high order Godunov fluxes to ensure solenoidal magnetic fields in magnetohydrodynamic simulations, J. Comput. Phys. 149 (1999) 270–292.
[27] D.S. Balsara, Divergence-free reconstruction of magnetic fields and WENO schemes for magnetohydrodynamics, J. Comput. Phys. 228 (2009) 5040–5056.
[28] C.W. Jiang, X.S. Feng, J. Zhang, D.K. Zhong, AMR simulations of magnetohydrodynamic problems by the CESE method in curvilinear coordinates, Sol. Phys. 267 (2010) 463–491.
[29] Y.F. Zhou, X.S. Feng, An improved CESE method and its application to steady-state coronal structure simulation, Sci. China Earth Sci. 153 (166) (2014).
[30] Y.F. Zhou, X.S. Feng, A new hybrid numerical scheme for two-dimensional ideal MHD equations, Chin. Phys. Lett. 27 (2010) 085201.
[31] C.L. Chang, Time-accurate local time stepping and high-order space–time CESE methods for multi-dimensional flows with unstructured meshes, in: 21st AIAA Computational Fluid Dynamics Conference.
[32] 蒋长锦, 科学计算和 C 程序集 (第一版), 中国水利水电出版社.
[33] S.T. Li, High order central scheme on overlapping cells for magnetohydrodynamic flows with and without constrained transport method, J. Comput. Phys. 227 (2008) 7368–7393.
[34] Thomas A. Gardiner, James M. Stone, An unsplit Godunov method for ideal MHD via constrained transport, arXiv:astro-ph/0501557v1, 25 Jan 2005.
[35] G.S. Jiang, C.C. Wu, A high-order WENO finite difference scheme for the equations of ideal magnetohydrodynamics, J. Comput. Phys. 150 (1999) 561–594.
[36] D.S. Balsara, Multidimensional HLLE Riemann solver: application to Euler and magnetohydrodynamic flows, J. Comput. Phys. 229 (2010) 1970–1993.